

University of New Orleans

ScholarWorks@UNO

University of New Orleans Theses and
Dissertations

Dissertations and Theses

Fall 12-16-2016

An Investigation Into the Origin, Composition, and Commercial Significance of a Sedimentary Subsalt Formation: Keathley Canyon, Gulf of Mexico

David Aaron Brassieur

University of New Orleans, New Orleans, david_brassieur@reagan.com

Follow this and additional works at: <https://scholarworks.uno.edu/td>



Part of the [Geology Commons](#), [Geomorphology Commons](#), [Geophysics and Seismology Commons](#), and the [Oil, Gas, and Energy Commons](#)

Recommended Citation

Brassieur, David Aaron, "An Investigation Into the Origin, Composition, and Commercial Significance of a Sedimentary Subsalt Formation: Keathley Canyon, Gulf of Mexico" (2016). *University of New Orleans Theses and Dissertations*. 2245.

<https://scholarworks.uno.edu/td/2245>

This Thesis is protected by copyright and/or related rights. It has been brought to you by ScholarWorks@UNO with permission from the rights-holder(s). You are free to use this Thesis in any way that is permitted by the copyright and related rights legislation that applies to your use. For other uses you need to obtain permission from the rights-holder(s) directly, unless additional rights are indicated by a Creative Commons license in the record and/or on the work itself.

This Thesis has been accepted for inclusion in University of New Orleans Theses and Dissertations by an authorized administrator of ScholarWorks@UNO. For more information, please contact scholarworks@uno.edu.

An Investigation Into the Origin, Composition, and Commercial Significance of a
Sedimentary Subsalt Formation: Keathley Canyon, Gulf of Mexico

A Thesis

Submitted to the Graduate Faculty of the
University of New Orleans
in partial fulfillment of the
requirements for the degree of

Master of Science
in
Earth and Environmental Sciences
Geology and Geophysics

By

David Aaron Brassieur

B.S. The University of New Orleans, 2013

December 2016

Copyright 2016, David Aaron Brassieur

DEDICATION

For
Henry and Wallace

ACKNOWLEDGEMENTS

Above all, I have the deepest gratitude for my wife Emilie and our two sons Henry and Wallace. Without their encouragement and support, I would not have been able to accomplish such an achievement.

Thank you Petroleum Geoservices (PGS) for an excellent seismic dataset making it possible to perform this study, and thank you Schlumberger, Petrel E&P software support team.

Many thanks to Dr. Juliette Ioup of the UNO Physics Department for her support and encouragement, and to my thesis committee members -- Mark Alan Kulp PhD and Michael G. Fitzgerald PhD.

Thank you Dr. Martin P.A. Jackson, UT Austin; senior research scientist Bureau of Economic Geology (BEG) ret., Dr. Michael R. Hudec, UT Austin; senior research scientist (BEG), and Dr. Tim P. Dooley, UT Austin; research scientist (BEG), for your support and encouragement.

Very special thanks to Dr. Selim S. Shaker of Geopressure Analysis Services in Houston, Texas. Dr. Shaker provided valuable insight into my petrophysical investigation sharing his time and professional experience.

Very special thanks to Brad A. Robison. Brad has shared the assemblage of an extraordinary professional career through his guidance and instruction.

TABLE OF CONTENTS

TABLE OF FIGURES	vi
TABLE OF GRAPHS.....	vii
TABLE OF TABLES	viii
ABBREVIATIONS	ix
ABSTRACT.....	xi
INTRODUCTION.....	1
OBJECTIVES.....	2
GEOLOGIC SETTING	3
SEDIMENTARY SUBSALT UNIT A	11
DATA and METHODS.....	16
CHAPTER 1 – SEISMIC STUDY.....	24
INTRODUCTION.....	24
SALT TECTONICS.....	24
CONCEPT	27
CONCLUSIONS.....	29
CHAPTER 2 – PETROPHYSICAL ASSESSMENT	35
INTRODUCTION.....	35
WELL-LOG PROCESSING	36
SALT.....	47
WELL CONTROL.....	49
CONCLUSIONS.....	55
REFERENCE.....	59
EQUATIONS.....	62
VITA.....	66

TABLE OF FIGURES

Figure 1. Northern Gulf of Mexico OCS region, blocks, and active leases	1
Figure 2. Early Triassic continental deployment.....	4
Figure 3. Early Jurassic continental deployment	5
Figure 4. Late Jurassic continental deployment	6
Figure 5. Sequential cross-section showing the evolution of the Gulf of Mexico.....	7
Figure 6. Differential sediment loading - conceptual schematic.....	7
Figure 7. Northern Gulf of Mexico with bathymetric contours.	8
Figure 8. Regional map with lease blocks from dataset	9
Figure 9. Geologic time scale	10
Figure 10. True vertical thickness map of Unit A.....	11
Figure 11. Dip oriented 2D seismic cross-section - Flat-and-ramp morphology	12
Figure 12. Dip parallel 2D seismic cross-section of Unit A	13
Figure 13. Asymmetric spreading of a salt sheet.....	13
Figure 14. Transport-parallel lineaments with dimensions.....	14
Figure 15. 3D model of Unit A.....	19
Figure 16. TPL physical dimensions	20
Figure 17. 3-D model showing zone of interest.....	21
Figure 18. Dip oriented 2D seismic cross-section with wiggle trace overlay	24
Figure 19. Dip-oriented 2D seismic cross section - cropped velocity model overlay.....	25
Figure 20. Conceptual schematic - gravitational instability	26
Figure 21. Evolution of a salt diapir	27
Figure 22. The evolution of diapiric piercement	28
Figure 23. Salt lobe coalescence	31
Figure 24. Salt lobe coalescence.....	33
Figure 25. Dip-oriented 2-D seismic cross-section - dirty salt	36
Figure 26. 3D model to 27,000 ft	37
Figure 27. Hydrocarbon maturity phase diagram.....	40
Figure 28. Borehole conditions 20 kft to 35 kft	43
Figure 29. Injectivity test	52

TABLE OF GRAPHS

Graph 1. Hydrostatic data	38
Graph 2. Corrected bulk density	39
Graph 3. Acoustic velocities.....	41
Graph 4. Drill bit dia./Caliper measure.....	42
Graph 5. Borehole conditions at	44
Graph 6. Drilling Tolerance Window (DTW)	45
Graph 7. Mud weight, Annular PWD ECD, and fracture pressure gradient	47
Graph 8. Leak off Test and Fracture Integrity Test	55
Graph 9. Composite petrophysical graph.....	56

TABLE OF TABLES

Table 1. Notable observations.	15
Table 2 Table of seismic deliverables	16
Table 3. Well log data deliverables for Tiber Well KC102.....	17
Table 4. Well log data deliverables for to Tiber_2 well KC57	18
Table 5. List of suture terms	32
Table 6. Formation integrity and Leak Off Tests.....	51

ABBREVIATIONS

1.	APLC: Neutron log curve
2.	BEG: Bureau of Economic Geology
3.	BHP: Bottom Hole Pressure
4.	BOEM: Bureau of Ocean & Energy Management
5.	BOS: Base of Salt
6.	BOUA: Bottom of Subsalt Unit A
7.	BSEE: Bureau of Safety & Environmental Enforcement
8.	BYA: Billion Years Ago
9.	CRS: Coordinate Ref. System
10.	DD: Drill Deck
11.	DF: Drill Floor
12.	DPHI: Density-Porosity log
14.	DTW: Drilling Tolerance Window
15.	ECD: Equivalent-Circulating Density
16.	FIT: Formation Integrity Test
17.	FP: Fracture Pressure
18.	FR: Flat-and Ramp morphology
19.	GB: Garden Banks protraction area
20.	GOM: Gulf of Mexico
21.	HLDS: Hostile Environment Litho-density Sonde log
22.	HS: Hydrostatic Pressure
23.	ISIP: Minimum formation fracture-extension pressure.
24.	KB: Kelly Bushing
25.	KC: Keathley Canyon
26.	LCAL: Caliper log
27.	LOC: Loss of Circulation
28.	LOT: Leak Off Test
29.	MD: Measured Depth
30.	ML: Mudline (seafloor)
31.	MW: Mud-weight
32.	MYA: Million Years Ago
33.	OB: Overburden Gradient
34.	OCS: Outer Continental Shelf
35.	PEFL (PEL): Photoelectric Effect
36.	PGS: Petroleum Geoservices
37.	PS: Max Principal Stress
38.	PWD: Performed While Drilling
39.	R ₁ – R ₆ : TPL ridges

40.	RHOM: Bulk Density Curve
41.	SB: Salt Buoyancy
42.	TD: Total Depth
43.	TOS: Top of Salt
44.	TPL: Transport-parallel lineaments
45.	TVD: True Vertical Depth
46.	UTM: Universal Transverse Mercator
47.	TOUA: Top of Subsalt Unit A
48.	V ₁ – V ₃ : TPL first order valleys
49.	V _A – V _E : TPL second order valleys
50.	WD: Water Depth
51.	WMUD: Mud-weight log
52.	ZOI: Zone of Interest

ABSTRACT

Sub-salt oil and gas formations in deep-water northern Gulf of Mexico are high priority targets. Advances in seismic processing allow for high-resolution, below-salt imaging. Understanding the modes of salt emplacement provide insight into sub-salt traps and potential drilling hazards.

A sub-salt sedimentary unit lies in the Keathley Canyon protraction. Salt lobe coalescence created the transport-parallel package of lineaments on the base of salt contact surface. In addition, variable sediment aggradation rates created ramps, flats, and basal cutoffs along the base of the allochthon as salt and sediment competed for space. Seismic models identify modes of salt emplacement, salt/sediment interactions, and mechanisms responsible for the morphology.

Petrophysical assessments highlight an abnormally pressured, dirty salt environment transitioning into a gouge zone. The dirty salt drilling environment adds an element of difficulty to managing borehole pressures, which dictates a unique mud-weight plan, designed for resisting formation pressures without fracturing the lithology below.

Keywords: Keathley Canyon (KC); diapirism; subsalt imaging; dirty/clean salt; mud-weight; formation pressure; gouge zone; hydrostatics; fracture gradient; salt tectonics; salt suture; allosuture; autosuture; subsalt sedimentary unit.

INTRODUCTION

The northern Gulf of Mexico (GOM) is a region commonly known for having an active hydrocarbon-industry presence. Commercially, the northern GOM is separated into three planning areas; Western, Central and Eastern, which are further separated into protraction areas (figure 1). Protraction areas are divided into numerous blocks each of which are 3 x 3 mi.

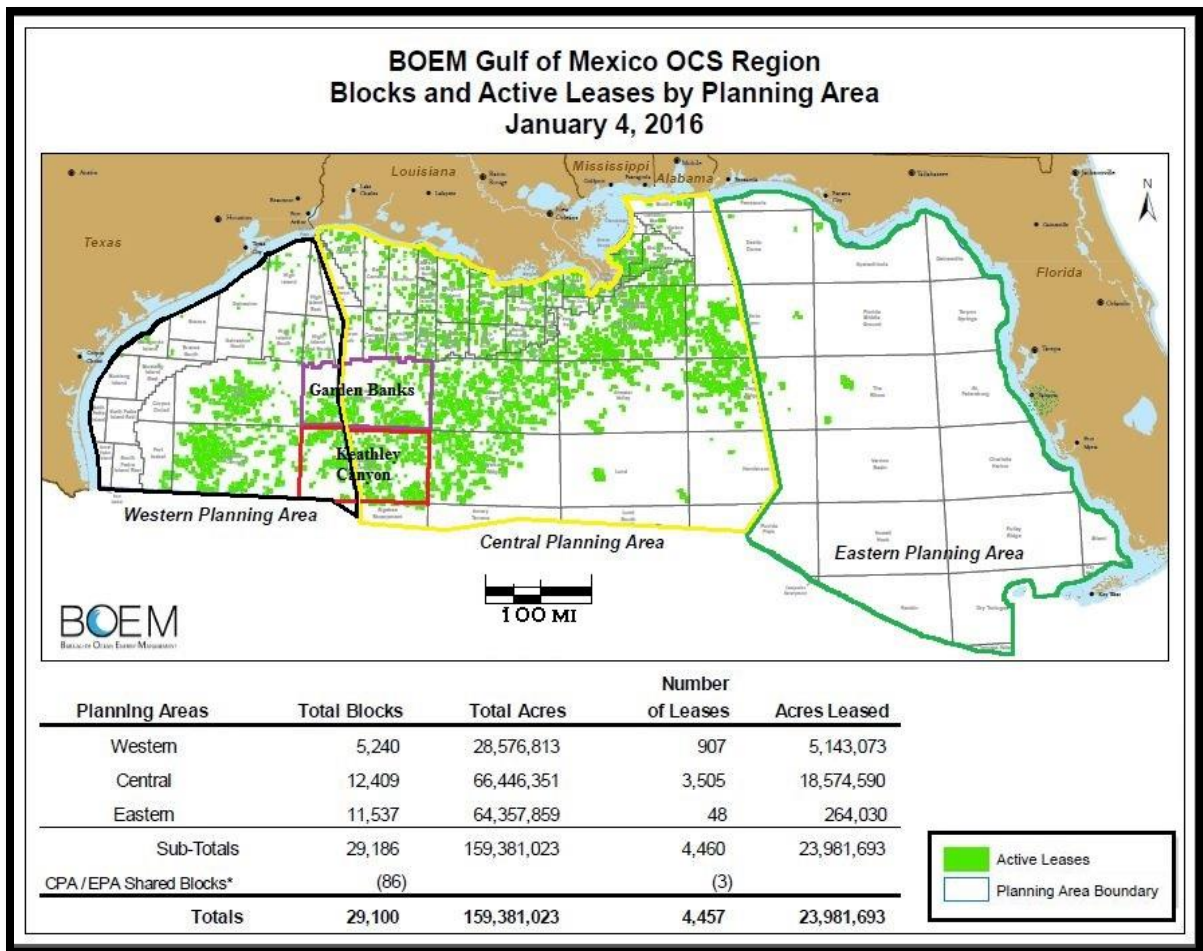


Figure 1. Northern Gulf of Mexico OCS region, blocks, and active leases by planning area. Western planning area: black border. Central planning area: yellow border. Eastern planning area: green border. Garden Banks protraction: purple border. Keathley Canyon protraction: red border. Figure modified from BOEM 2016 active lease map

Subsalt oil and gas formations in deep-water are high priority targets due to advances in subsalt seismic imaging. Interpretation of high-resolution, below-salt seismic data helps identify the location and condition of sub-salt formations and traps. In this study, below salt seismic interpretations of an Oligo-Miocene formation assess the modes of salt emplacement finding them consistent with models seen in (Jackson et al., 1994).

OBJECTIVES

The two principal objectives of this study are (Ch.1) seismic interpretation and (Ch.2) petrophysical assessment of a sedimentary subsalt unit hereafter referred to as Subsalt Unit A. The upper surface of this unit contacts the base of a nearly 17,000 ft thick allochthonous salt nappe, and the base is stratigraphically above a 300 ft thick Oligocene sand.

The first objective of this study implements seismic interpretation techniques for defining modes of salt emplacement, salt interaction with depositing sediments, and mechanisms responsible for the morphology of this basal salt contact. The second objective is a petrophysical assessment designed to verify if the poorly striated seismic reflections (gouge zone) seen in 2D seismic cross-sections are accurate representations and not seismic artifact, and to investigate formation fluid pressure and fracture gradients throughout the wellbore.

Gouge zone (Shaker, 2008) is an industry term used interchangeably with Rubble zone (Saleh, et al., 2013) and Gumbo zone (House and Pritchitt, 2010). Here, these terms reference BOS formations (zones) containing transported and crumbled sediments. These zones have potential to present drilling hazards such as abnormal formation pressures and/or fracture gradients, and may be heavily fluidized. Understanding drilling hazards before drilling will help with the design of a safe and productive drilling operation. This assessment of drilling reports, seismic data, and well logs will produce a comprehensive understanding of Subsalt Unit A with additional discussion on the management of potential drilling hazards when operations drill through the base of thick tabular salt.

GEOLOGIC SETTING

The continuously evolving subsalt play in the GOM is connected with the geologic history of the supercontinent Pangea; including the pre-rifting and rifting phases in the Late Triassic and Jurassic periods or Late Paleozoic and Early Mesozoic eras (figures 2, 3, 4, & 9). Approximately 240 million years ago, during the Early Triassic and prior to the gulf's existence, the supercontinent Pangea was principally assembled (figure 2). In the Early Jurassic, North America separated from Africa and South America, and by the Middle Jurassic, the Yucatan hanging wall separated from the North American plate (figure 3). A volcanic upper mantle extension began to push up creating new oceanic crust (Pendell & Kennan, 2007). The tectonic activity that emanated would eventually construct the GOM basin influencing the distribution of infilling

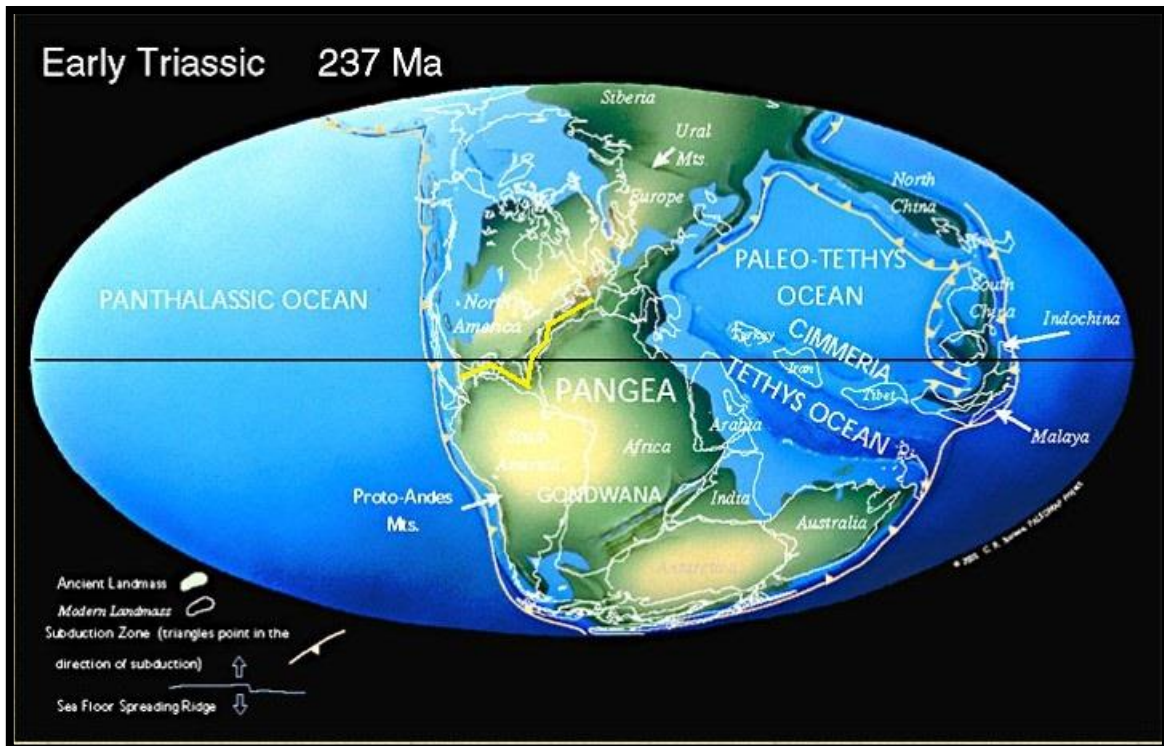


Figure 2. Early Triassic continental deployment. Yellow line indicates location of rift zone. Figure modified from the Scotese paleogeographic map project (Scotese, 2001).

sediments (figure 4). The extensional tectonics deformed the continental crust resulting in grabens and rift basins that became filled by non-marine sediments and volcanics. (Buffler and Sawyer, 1985; Pindell, 1994; Salvador, 1987). Stern and Dickinson (2010) hypothesized the GOM as a back arc basin and spreading center resulting from the late Paleozoic to early Mesozoic rifting event (240 – 200 mya). They described the North American plate pulling away from the South American and African plates, and how subduction-related tectonism along the western margin of the North American plate permitted sporadic encroachment of the Pacific Ocean. Between these surges of encroachment, the connection with the Pacific Ocean would close, leaving behind an isolated body of saline ocean water (Stern and Dickenson, 2010). Detailing how the back arc basin grew behind the Nazas arc, which formed due to an eastward dipping subduction zone in

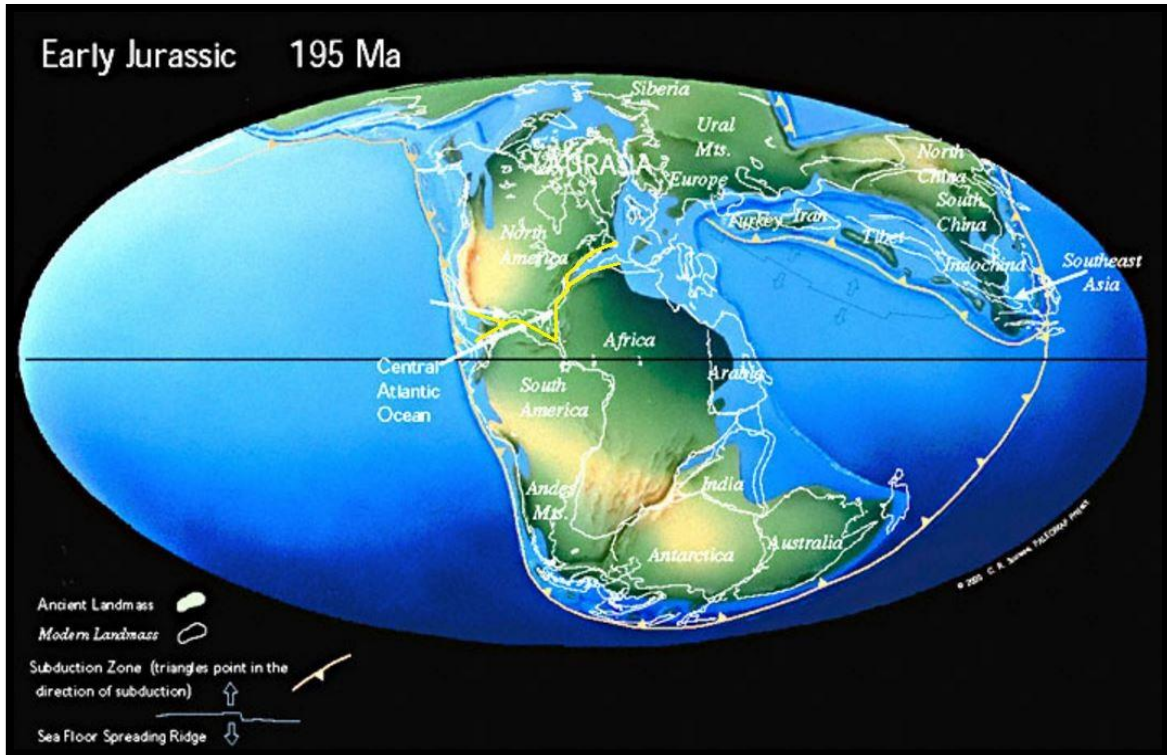


Figure 3. Early Jurassic continental deployment. Yellow line indicates location of rifting. Figure modified from the Scotese paleogeographic map project (Scotese, 2001).

the Late Jurassic, they indicated the main period of rifting as having occurred during the Middle Jurassic, and suggests that oceanic spreading continued into the Late Jurassic.

Tertiary progradation of sediments shed from orogenic events on the western margin of the GOM fill the subsiding basin. Widespread salt tectonism and differential sediment loading account for large variations in sediment patterns and structural style in the GOM (Bryant et al., 1990). The rift architecture of the GOM provided the complicated basement fabric for the deposition and movement of autochthonous (deposited in its present position) and subsequently allochthonous (deposited in a location other than its present position) salt bodies. The crust separating the Yucatan platform from the North American plate (figure 6) stretched, dissecting the salt body into two large regions in the northern and southern GOM (Humphris, 1978;

Salvador, 1987; Buffler, 1989). The salt, when remobilized later, played a critical role in the maturation, migration, and entrapment of hydrocarbons in the northern GOM Basin (Buffler, 1991). The GOM is presently a tectonically passive sedimentary basin with a remarkably complex and heterogeneous continental slope.

An extremely important geologic event associated with GOM-rifting was the thick deposition of Louann salt across the basin. Halite-NaCl is commonly known as salt or rock salt which is a water-soluble halide mineral and evaporite (Klein et al. 2008). Jackson (1997) defines an evaporite as a water-soluble mineral sediment resulting from concentration and crystallization by evaporation from an aqueous solution.

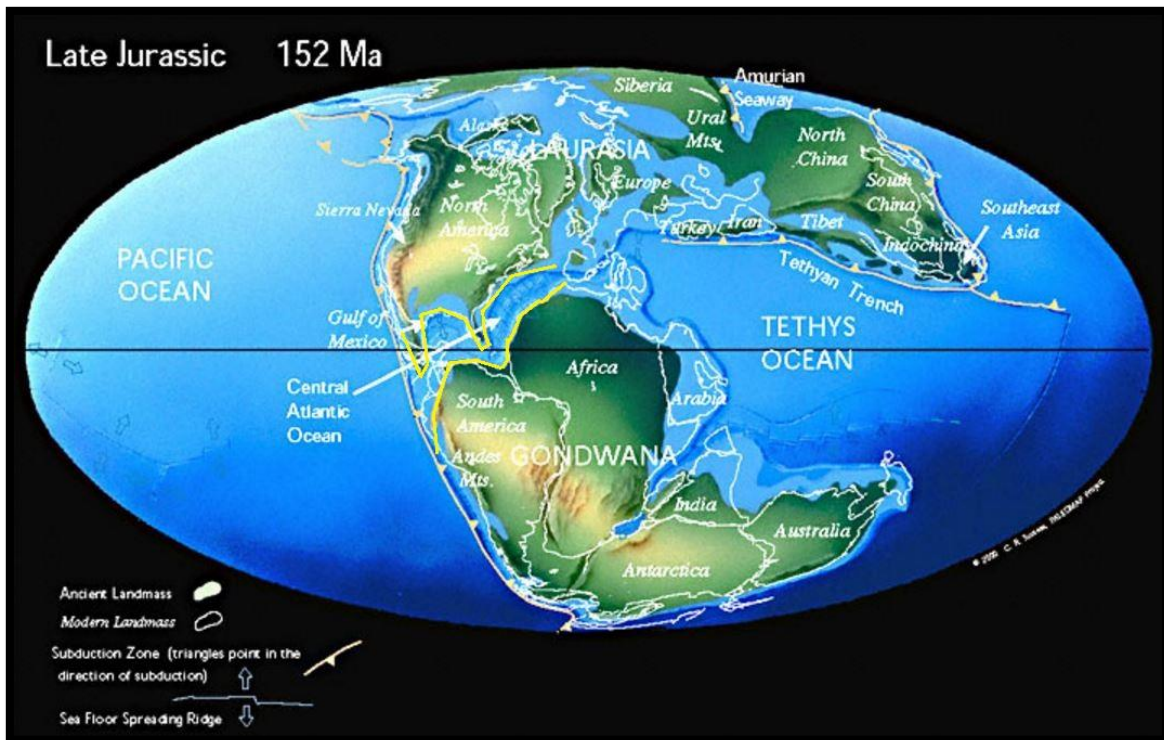


Figure 4. Late Jurassic continental deployment. Yellow indicates zone of rifting. Figure modified from the Scotese paleogeographic map project (Scotese, 2001).

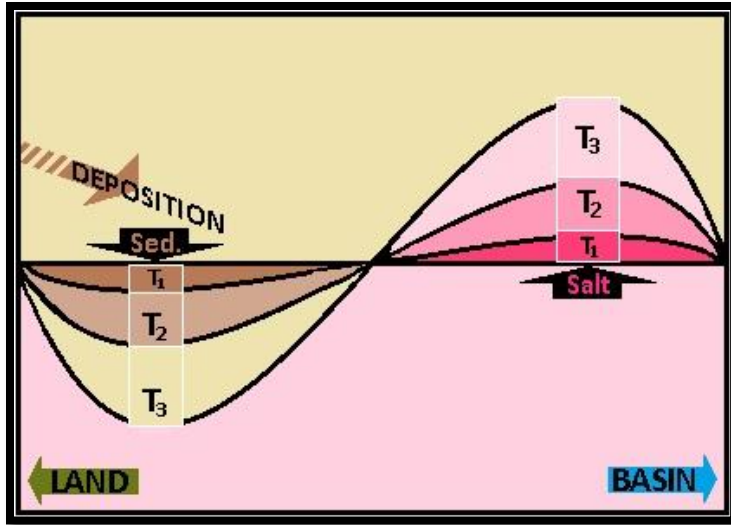


Figure 5. Differential sediment loading conceptual schematic diagram. Salt: pink hues, sediment: brown hues. The horizontal black line separating sediment from salt represents T-0. T-1, 2, and 3, correlate relative time for the tops of sediment and salt surfaces. Positive Feedback Loop: As sediments accumulate, the resultant overburden forces push down onto the salt causing the salt to rise. Sediments subside creating accommodation space for additional sediments to deposit. Salt rises and is unable to accommodate sediment collection. Figure created using MS tools.

A regulated basin environment where the seawater input rate remains less than the rate of water evaporation is necessary for supersaturation and precipitation to occur. In the Middle Jurassic, seawater entered the GOM and through countless cycles of seawater evaporation and replenishment, these regulated/restricted bodies of water became supersaturated

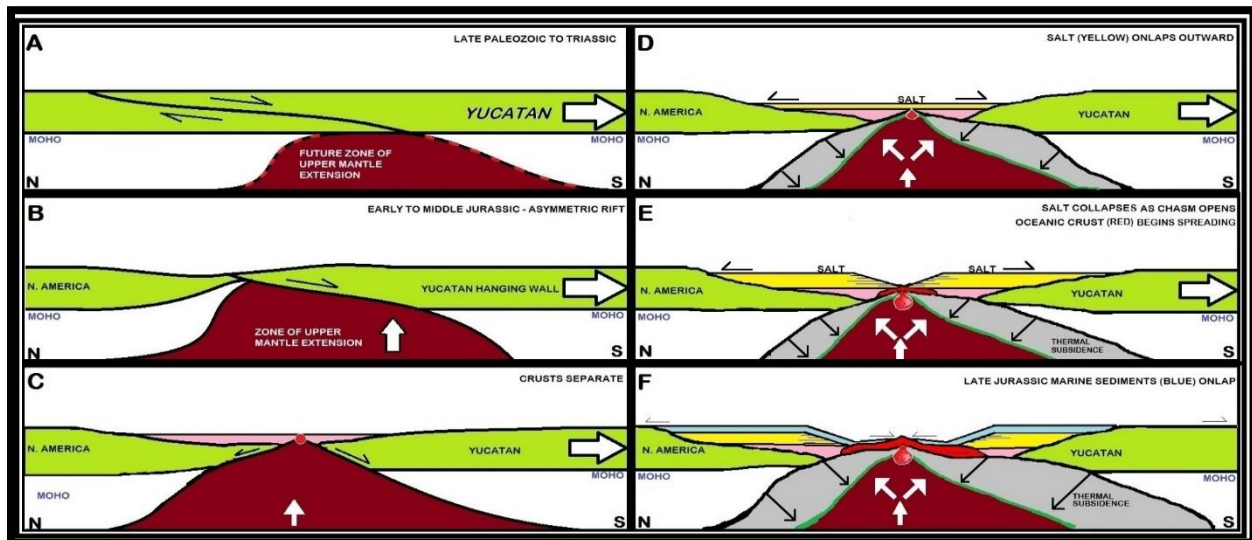


Figure 6. Sequence of cross-sections depicting the rift evolution of the Gulf of Mexico. A-C: from onset of asymmetric rifting to the transition to proto-ocean crust formation. D-F: Depicts the transition from subsalt emplacement of proto-ocean crust in the central Gulf to true submarine emplacement of typical ocean crust no earlier than the Middle Oxfordian time. Figure modified from Pendell and Kennan, Gulf of Mexico Salt, GCSSEPM (2007).

resulting in halite precipitation within the hypersaline basins. The precipitated halite crystals congregated in the vast accommodation space created by local subsidence.

In *The Prize Beneath the Salt*, seismic data reveal that the Louann Salt varied in thickness from almost zero to perhaps as much as 2.5 mi as it accumulated on a surface made uneven by faulting, erosion or volcanism (Dribus, et al. 2008). This salt, when remobilized later, played a critical role in the maturation, migration, and entrapment of hydrocarbons in the northern Gulf Basin (Buffler, 1991). Sediment loading drives salt migration from above forcing the salt to interact with the surrounding sedimentary units. There are two prevalent schools of thought on the migration of salt in the GOM. Deigel et al. (1995) and Fiduk et al. (1999) contend that the salt

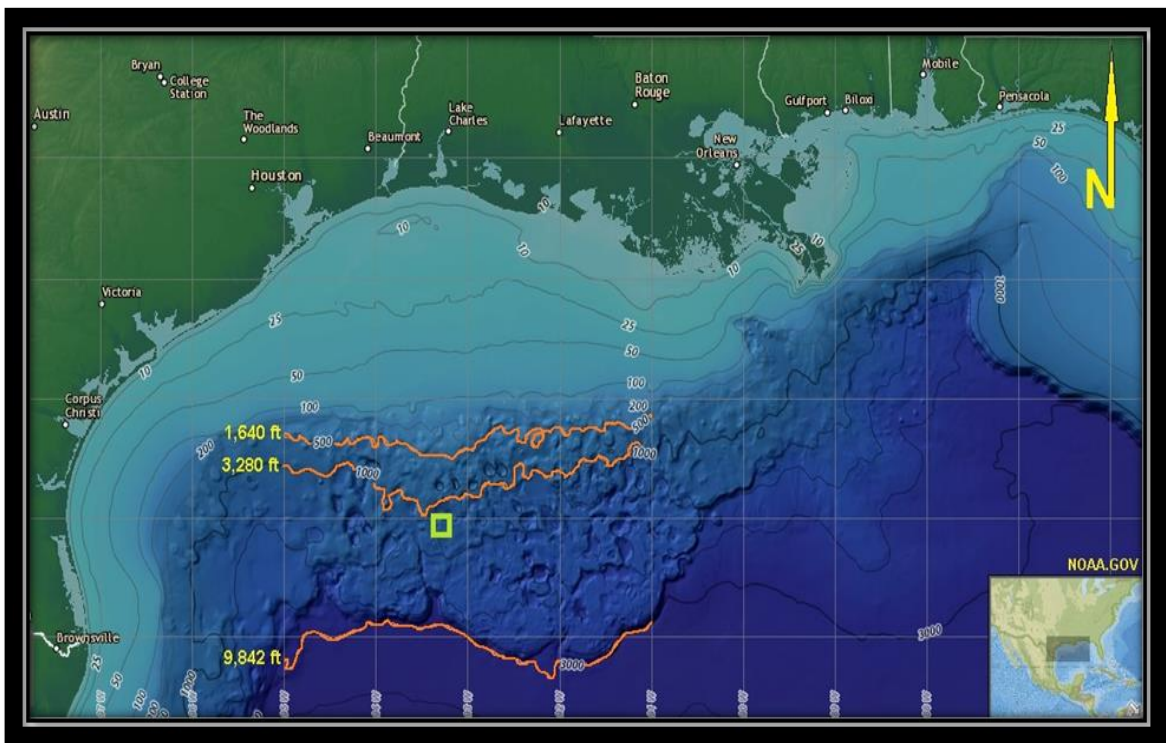


Figure 7. DEM color shaded relief imagery of Northern Gulf of Mexico with bathymetric contours. Study location; green box. Orange depth contours from top to bottom at 500, 1,000, and 3,000 meters. Depth conversions to feet in yellow. Figure modified from NOAA.gov relief imagery, 2016.

undergoes generalized movement from differential sediment loading into the basin over time. In contrast, Wu et al. (1990) believe that the basinward movement of salt was in response to up-

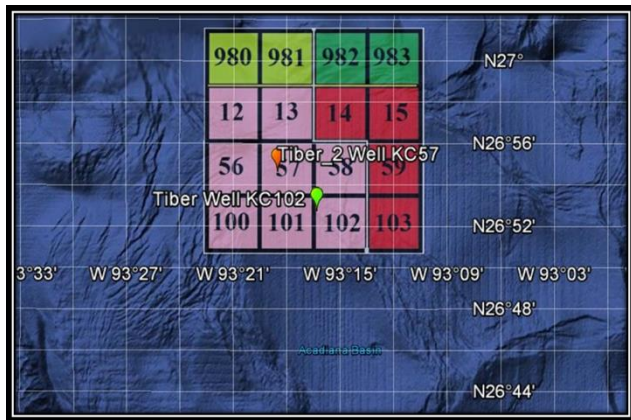


Figure 8. Regional map with overlay of lease blocks from dataset. Green shades are Garden Banks Protraction. Red shades are Keathley Canyon Protraction. Darker hues are central planning area and lighter hues represent western planning. Image created using Google Earth and MS tools.

dip depositional loading. Regardless, localized differential loading became dominant once the salt highs and lows were established. In order to visualize the differential sediment loading, consider an increased overburden force on the salt lows where sediment accommodation is higher as opposed to the lesser force on salt highs, which lack the accommodation for sediment collection (figure 5).

This analysis utilizes seismic data covering 16 contiguous blocks (4x4) within the Keathley Canyon (KC) and Garden Banks (GB) protractions and the Western and Central planning areas in a water depth greater than 4000 ft (figure 7). The two wells in this dataset are Tiber Well in KC102 and Tiber_2 Well in KC57 (figure 8). These wells are located approximately 50 mi north of the Sigsbee Escarpment, which is the terminal limit of the allochthonous salt bodies that have been migrating in a southeastern direction in this area (Trudgill, 1999). Nearly 225 mi south of Lake Charles, Louisiana, the KC protraction covers approximately 8,500 mi², and is home to various oil exploration and development operations. Of the two wells in this study, Tiber Well in KC102 was the first drilled (2009) with well log data becoming public in 2011. The Deepwater Horizon drilled Tiber with the objective of contacting the Wilcox formation at a depth of ~28,000

ft to ~32,000 ft as a hydrocarbon reservoir, and continuing below the Cretaceous (total depth-TVD 35,055 ft) for the purpose of locating and evaluating source rock material. Investigation of the Halliburton drilling reports indicates that the original target depth was probably a deeper (+/-

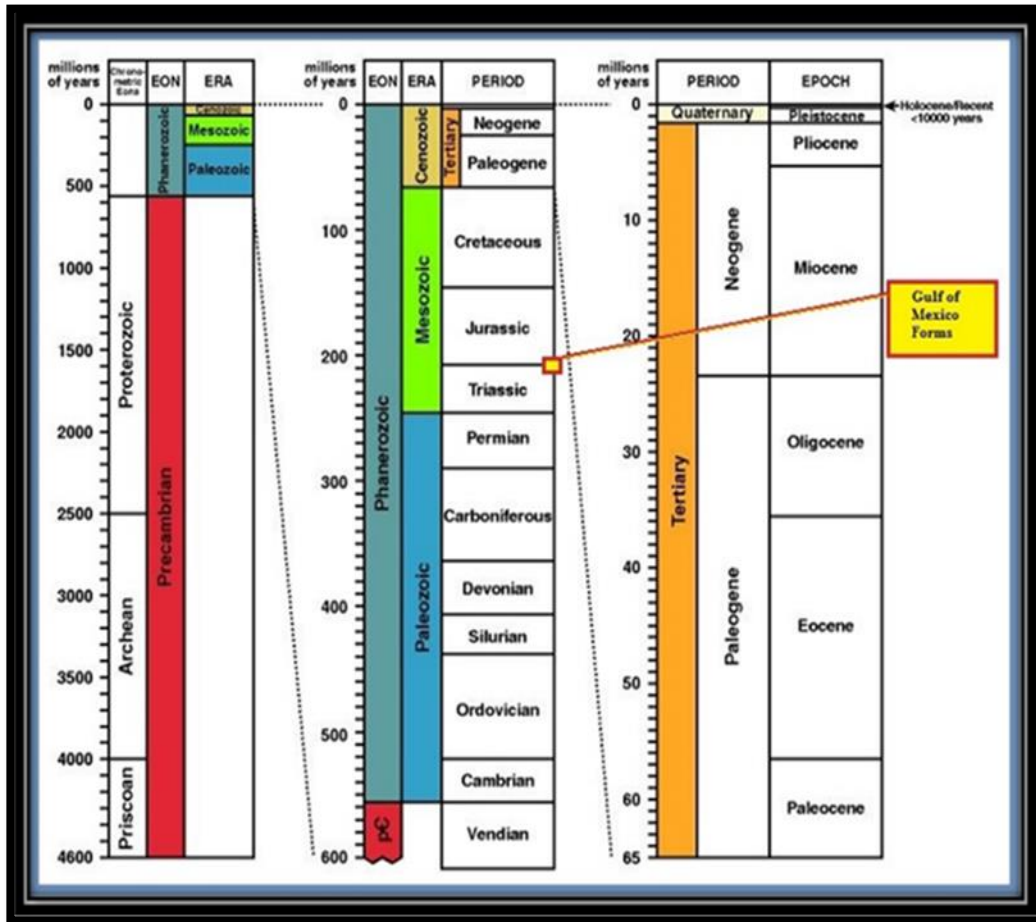


Figure 9. Geologic time scale for all of Earth’s history. Yellow text box indicates Early Jurassic rifting of Pangea. Figure modified from U. Calgary Geo-timescale.

37,000 ft), unreached target. There were bore hole problems in the form of Lost Circulation materials (LCM) at total depth (TVD) supporting this theory. Tiber_2 KC57 Well was drilled in 2013-14 and well log data became public in 2016. Tiber_2 KC57 is located 3.6 mi northwest of Tiber Well KC102, penetrated to a depth of 31,250 ft, and passed through similar environments for the same purposes.

SEDIMENTARY SUBSALT UNIT A

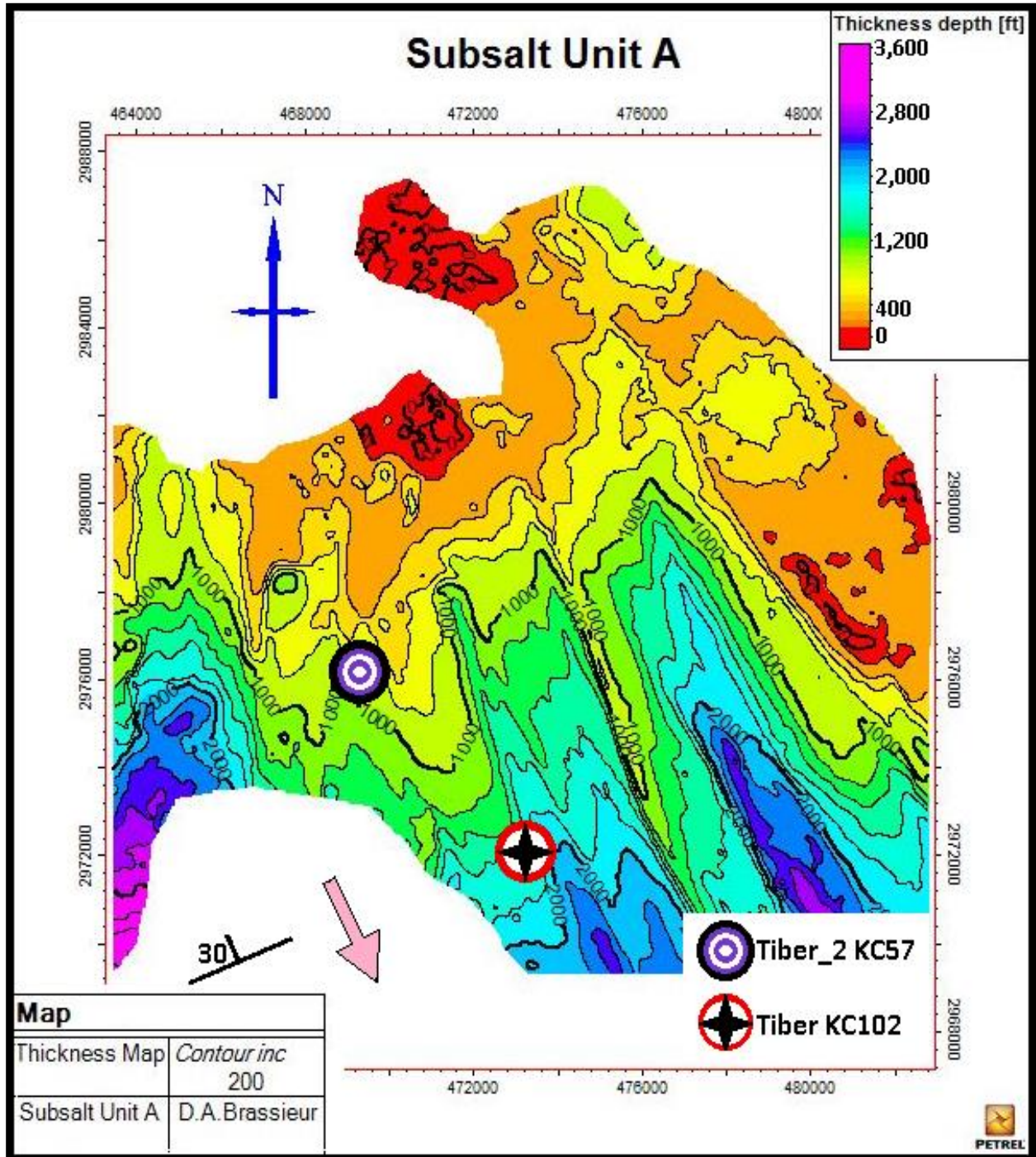


Figure 10. True vertical thickness depth map of Subsalt Unit A showing wells Tiber and Tiber_2. Generalized direction of salt emplacement in the northern GOM identified with pink arrow. True vertical thickness depth in ft MD. Figure created using Petrel 2013 E&P.

At Tiber Well KC102, the measured depths (MD) to: mudline (ML), top of salt (TOS), base of salt (BOS), and the upper/basal surfaces of Subsalt Unit A are listed at 4,207 ft, 8,480 ft, 24,980 ft, 25,000 ft, and 26,350 ft respectively. A thickness map for Unit A (figure 10) illustrates the contact surface morphology, true vertical thickness, and regional orientation of the unit.

Subsalt Unit A is a ramp-shaped, subsalt sedimentary unit with an angled upper surface contacting the base of a large, allochthonous salt nappe. The ramp geometry strikes northeast with a northwest-facing 30° dip angle (figure 11). When viewed in dip-oriented 2-D seismic cross-sections (figures 11 & 12), the contact surface exhibits a classic flat-and-ramp morphology consistent with passive phases of diapiric piercement (figure 12), and a poorly striated seismic

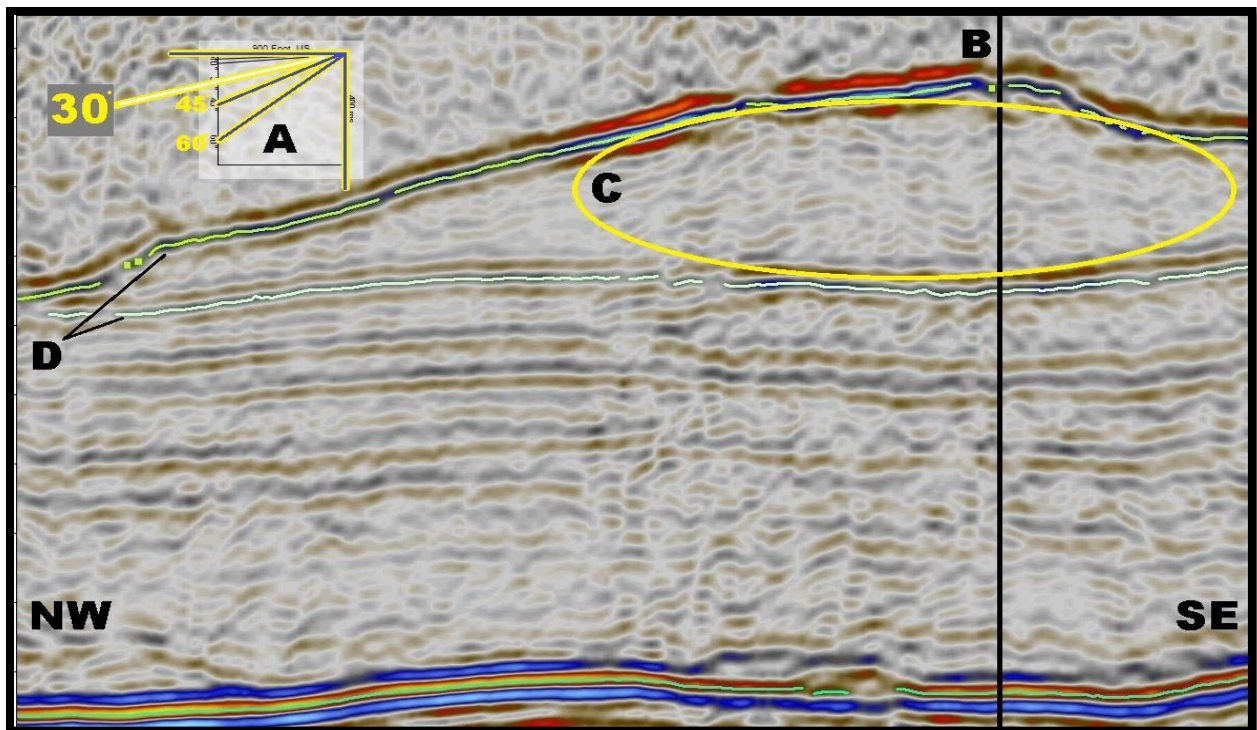


Figure 11. Dip parallel 2D seismic cross-section of Subsalt Unit A showing ramp angle, and the poorly striated seismic reflections within. The Petrel protractor attribute (A) indicates a ramp angle at ~30° (protractor accounts for vertical exaggeration). Black vertical line (B) represents Tiber Well KC102. Poorly striated reflections within the unit (C). Upper and lower interpreted horizons (D) Figure created using Petrel 2013 E&P.

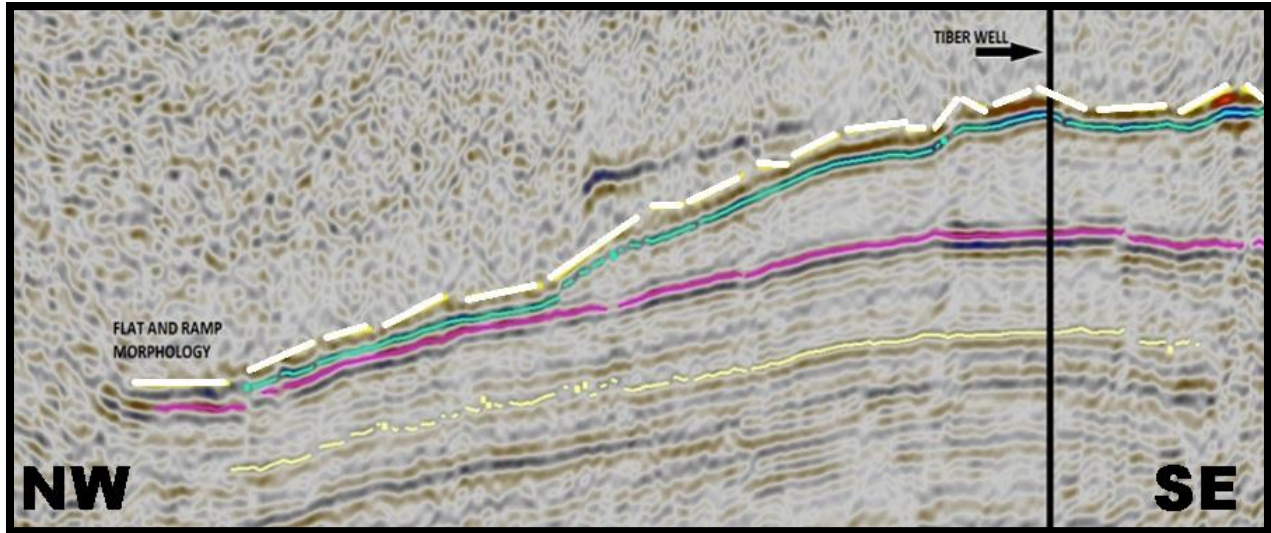


Figure 12. Dip oriented 2D seismic cross-section of Subsalt Unit A. Flat-and-ramp morphology indicated with white bars. Tiber well path indicated by black vertical line. Figure created using Petrel 2013 E&P.

reflection profile (figure 11c) consistent with gouge zones. When in strike-oriented cross section, the contact surface exhibits a large transport-parallel package of lineaments (TPL) that are consistent with basal sutures (figures 13 & 14).. Table 1 lists the notable observations of Subsalt Unit A.

The TPL are the high ridges and deep valleys labeled east to west R₁ through R₆, V₁ through V₃, and V_A through V_E, (figure 14B.) Within the limits of this dataset and from the same

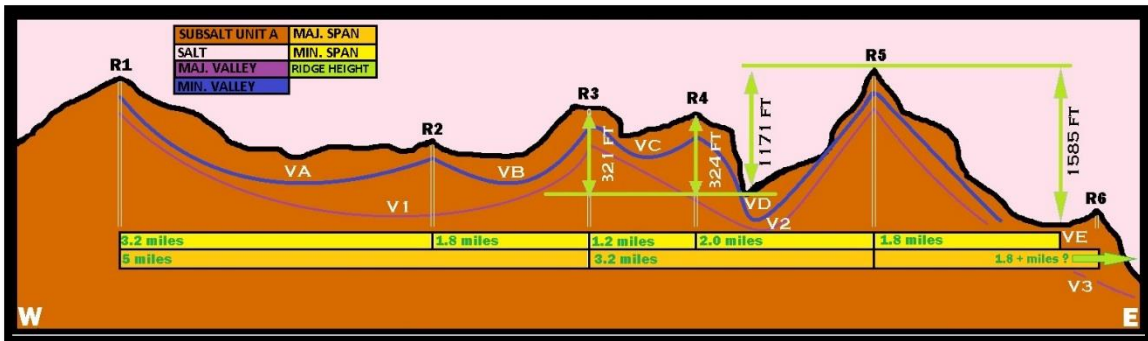


Figure 13. TPL of Unit A with peak-to-peak (horizontal) and peak-to-valley (vertical) measurements. Figure created using MS tools.

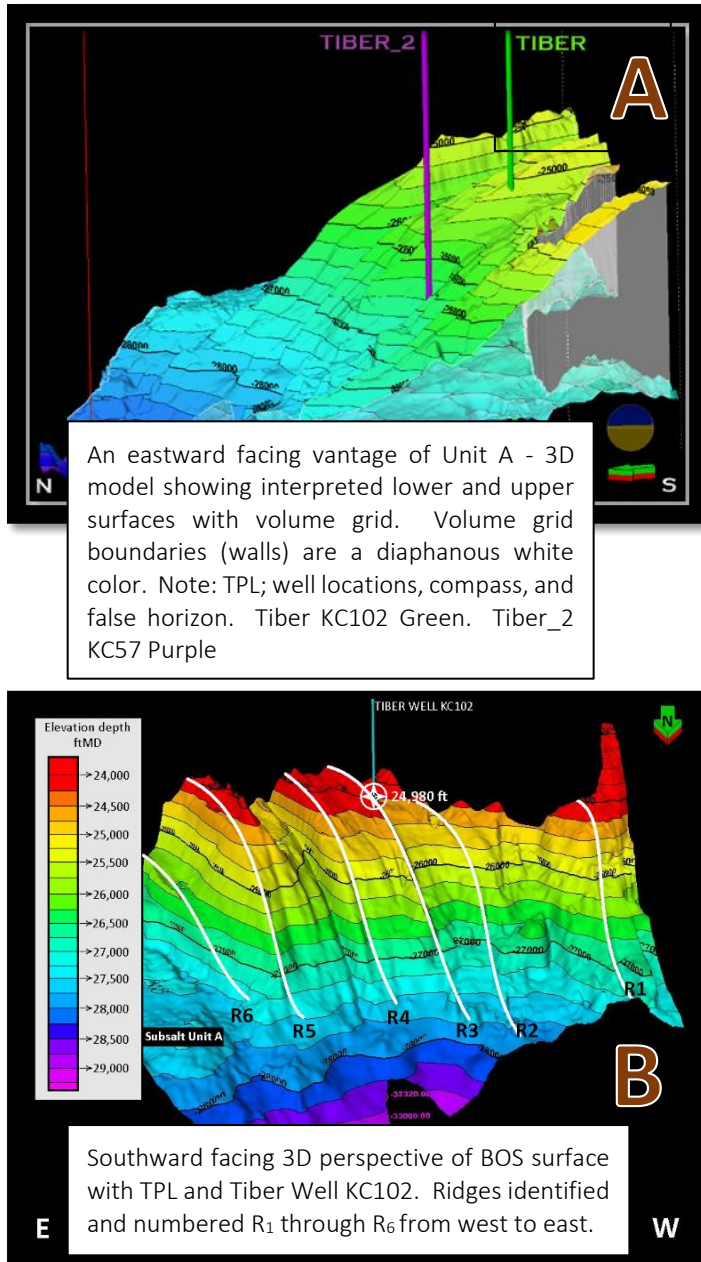


Figure 15. 3D models of Subsalt Unit A showing depth, well locations (A), and upper surface morphology (B). Figures created using Petrel 2013 E&P.

perspective, there are three first order valleys (V_1 , V_2 , and V_3), five second order valleys (V_A , V_B , V_C , V_D , & V_E), and six first order ridges (R_1 through R_6) (figure 13). The first order valleys V_1 , V_2 , and V_3 belong to ridges R_1 to R_3 , R_3 to R_5 , and from R_5 to R_6 respectively. The second order valleys V_A through V_E span sequentially across the Ridges from R_1 to R_6 . R_6 may not be the easternmost limit of V_3 and may be a second order ridge. R_6 is a substantial peak at approximately 300 ft of vertical relief from the lowest point in V_3 to the peak at R_6 . This dataset terminates east of R_6 and without additional processed seismic data, one can only speculate on the morphology of Subsalt Unit A outside of the 16 blocks comprising

this study. Although major valley V_3 is cutoff by the easternmost limit of seismic data, R_6 is recognized as a second order ridge and part of a major valley (V_3) beginning with R_5 and ending at R_{6+n} where n is the number of high order ridges between R_6 and the next major ridge R_n . The

three major valleys were measured peak to peak with V_1 spanning 5 mi and V_2 spanning 3.2 mi. V_3 is measured from peak R_5 to the limit of data spanning 1.8 mi. The 1.8 mi for V_3 is not a peak-to-peak measurement and has potential to span ≥ 3.6 mi.

Notable observations - SUBSALT UNIT A

1. Flat-and-ramp geometry of the salt contact or upper surface (figures 12 & 13).
2. Angular termination against base of salt. Upper surface dips at approximately 30° in a northwest-southeast direction.
3. Dip direction is parallel to the inferred direction of allochthonous salt migration for this region.
4. The upper, or salt contact surface, displays a, transport-parallel package of lineaments.
5. In contact with the base of dirty salt as a gouge zone whose reflections are minimally striated when viewing dip-oriented 2D seismic cross sections (figure 11)

Table 1. Notable observations of Subsalt Unit A with brief descriptions.

DATA and METHODS

SEISMIC DELIVERABLES	
PRODUCTS LICENSED and DELIVERABLE	DEFINITIONS
SEG-Y tape of Beam Stack (Enhanced)	Filtered and Scaled - <i>F/S</i>
SEG-Y tape of WEM Stack <i>F/S</i> (Filtered and Scaled)	Post-Stack Time Migration - <i>PostSTM</i>
SEG-Y tape of KPSDM Stack <i>F/S</i> _Filtered and Scaled)	Pre-Stack Depth Migration - <i>PTSM</i>
SEG-Y tape of Final Velocity Model	Kirchhoff Pre-Stack Depth Migration - <i>KPSDM</i>
Exchange format (UKOOA) tape of bin center map	Wave Equation Migration - <i>WEM</i>
	File format developed by SEG - <i>SEG-Y</i>
DEPTH / FORMAT	American Standard Code: Info. Interchange - <i>ASCII</i>
KPSDM Stack <i>F/S</i> / SEG-Y	High Definition Digital - <i>HDD</i>
WEM Stack <i>F/S</i> / SEG-Y	Society of Exploration Geophysicists - <i>SEG</i>
Beam Stack, Enhanced / SEG-Y	
Final Velocity Model / SEG-Y	DESCRIPTION OF SEISMIC DATA
Top and Base of Salt Horizons / ASCII	DW11-4_BEAM Stack Enhanced
	DW11_KPDSM: Kirchhoff Pre-Stack Depth Migration
	DW4_KPSDM: Kirchhoff Pre-Stack Depth Migration
	DW11-4_WEM: Wave Equation Migration

Table 2 Table of seismic deliverables with simple description. Seismic data supplied by PGS Marine Geophysical in Houston, Texas.

The dataset for this study consists of 16 blocks in the central planning area, including; KC 12-15, KC 56-69, KC 100-103 and blocks GB 980-983. Additionally, published well and drilling data for the two KC wells were purchased from BSEE (Bureau of Safety and Environmental Enforcement). The two wells are identified as Tiber well (OCS-G 25782 001 ST00BP00) in KC102 and Tiber_2 well (OCS-G 25777 001 ST00BP00) in KC57. All seismic files were loaded into Petrel 2013 E&P platform on a workstation and functionally tested to ensure proper loading of seismic data (table 2). Data references were set to coordinate reference system (CRS) NAD27 UTM Zone 15M, and all units of depth were converted to ft. Petrel is a Schlumberger-owned E&P software platform designed for the interpretation of seismic data, well correlations, reservoir modeling

TIBER KC102 WELL DATA

Description	Type	Designer
Mudlog	Report	Halliburton- SPS LWD
Directional Survey (x2)		
Combinable Magnetic Resonance	5 inch	Schlumberger Well Surveying Corp.
(MWD) AGR EWR M5	5 inch	Halliburton- SPS LWD
TVD (MWR) AGR EWR M5	5 inch	Halliburton- SPS LWD
TVD Array Induction-Density	5 inch	Schlumberger Well Surveying Corp.
Array Induction-Density	5 inch	Schlumberger Well Surveying Corp.
VISION Resistivity-Dual Frequency	5 inch	Schlumberger Well Surveying Corp.
Dipole Shear sonic Imager	5 inch	Schlumberger Well Surveying Corp.
Elemental Capture Spectroscopy Sonde	5 inch	Schlumberger Well Surveying Corp.
Gamma Ray Log	5 inch	Schlumberger Well Surveying Corp.
Hostile Natural Gamma Ray	5 inch	Schlumberger Well Surveying Corp.
Oil Based Imager Dual Image Log	5 inch	Schlumberger Well Surveying Corp.
(MWD) Resistivity-Blended	5 inch	Schlumberger Well Surveying Corp.
Oil Based MicroImager Gield Dips and Images	5 in, 1 in	Schlumberger Well Surveying Corp.
(MWD) Perform APWD_Time	2 inch	Schlumberger Well Surveying Corp.
(MWD)Bi-Modal Acoustic Processed Log	2 inch	Halliburton- SPS LWD
(MWD) AGREWR-M5-PWD-DIR	1 inch	Halliburton- SPS LWD
TVD (MWR) AGREWR-M5-PWD-DIR	1 inch	Halliburton- SPS LWD
ARRAY INDUCTION	1 inch	Schlumberger Well Surveying Corp.
TVD Array Induction Correlation Log	1 inch	Schlumberger Well Surveying Corp.
Borehole Profile	1 inch	Schlumberger Well Surveying Corp.
(MWD) Resistivity-Blended	1 inch	Schlumberger Well Surveying Corp.
Modular Formation Dynamics Tester	180 in	Schlumberger Well Surveying Corp.
Mechanical Sidewall Coring Tool	180 in	Schlumberger Well Surveying Corp.

Table 3. Well log data deliverables for Tiber Well KC102. Well data purchased from BSEE – The Bureau of Safety and Environmental Enforcement.

and simulation, volume calculations, and map construction, to maximize hydrocarbon reservoir development.

Utilizing a 3-D Kirchhoff pre-stack, depth-migrated seismic dataset provided by PGS Marine Geophysical, this survey comprises seismic data consisting of four sources and ten streamers. Seismic collection was completed in July of 1999, transecting in an East/West direction at 82 ft intervals and to nine seconds below mudline (seafloor). The Kirchhoff migration has been a staple of pre-stack seismic imaging for more than a decade. It incorporates time and

depth migration methods within a single basic program, facilitates target-oriented migration, and enables straightforward migration velocity analysis.

This workflow began by interpreting notable and primary seismic reflections (Mudline, Top of salt, Base of salt). Horizons were primarily chosen using 3-D seeded auto tracking (all inline and x-line) and guided auto tracking (individual inline or x-line) tool functions within the Petrel E&P seismic interpretation processes category. Mis-ties and discrepancies involving inline and cross-line interpretations were corrected manually utilizing a high-resolution viewport configuration to ensure correlative precision. Next, each corrected seismic horizon was converted into polygons and surfaces. Horizon surfaces were assigned an appropriate color/depth legend and depth contours. At this stage, a low pass filter was applied to the surfaces

TIBER_2 KC57 WELL DATA		
Well log	description	Originator
Mudlog		Haliburton - SPS LWD (full drillers report)
Directional Survey		Schlumberger Well Surveying Corp.
MWD Drilling Mechanics	5 inch	Schlumberger Well Surveying Corp.
Gamma Ray Log	5 inch	Schlumberger Well Surveying Corp.
(MWD) Perform APWD_Time	2 inch	Schlumberger Well Surveying Corp.
Borehole Profile	1 inch	Schlumberger Well Surveying Corp.
Array Induction Neutron Density	5 inch	Schlumberger Well Surveying Corp.
Ultrasonic Imager Tool	5 inch	Schlumberger Well Surveying Corp.
TVD (MWD) VisionResistivitySonic	5 inch	Schlumberger Well Surveying Corp.
TVD (MWD) VISION Resistivity	1 inch	Schlumberger Well Surveying Corp.
(MWD) Perform APWD_Time	2 inch	Schlumberger Well Surveying Corp.
Ultrasonic Imager Tool	5 inch	Schlumberger Well Surveying Corp.
SonicScannerDeltTCompandShear	1 inch	Schlumberger Well Surveying Corp.
(MWD) Perform APWD_Time	2 inch	Schlumberger Well Surveying Corp.
(MWD) Perform APWD_Time	2 inch	Schlumberger Well Surveying Corp.
(MWD) Perform APWD_Time	2 inch	Schlumberger Well Surveying Corp.

Table 4. Well data deliverables pertaining to Tiber_2 well KC57 purchased from BSEE - Bureau of Safety and Environmental Enforcement.

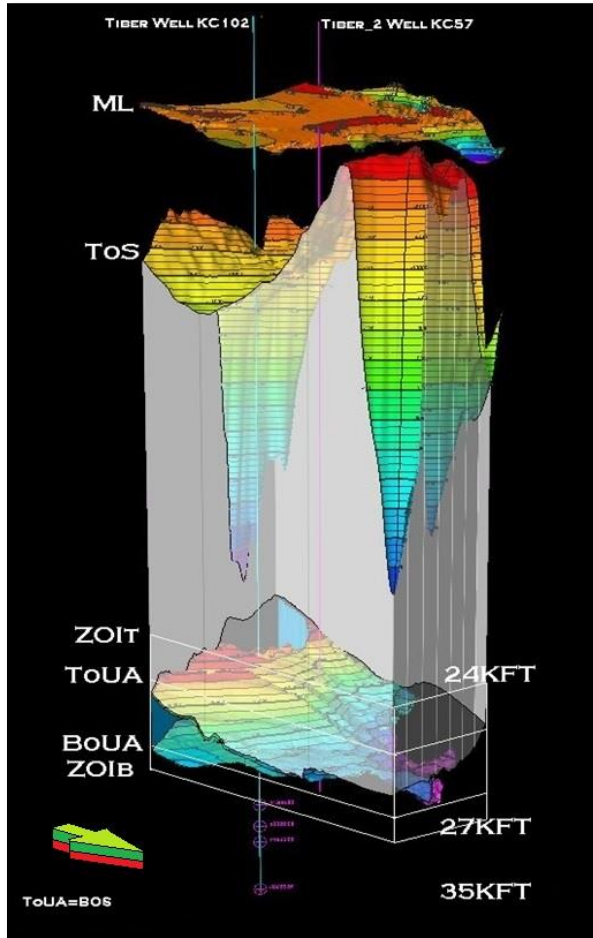


Figure 16. 3-D model showing the Tiber wells and the zone of interest. Depths are ft MD from Tiber Well KC102. Mud-line (ML), top of salt (TOS), base of salt (BOS)/top of Unit A (TOUA), base of subsalt unit A (BOUA), and zone of interest base (ZOIB). Figure created using Petrel E&P 2013.

for a smoothing effect, removing any outlier spikes or cones from the surfaces. Next, a zone of interest was identified and constituent horizons were processed using the same methods. This workflow allowed for the creation of 3-D models, grids, and volumes, each of which originated from the created horizon surfaces within the Petrel software (figure 15).

After seismic interpretation and modeling of the seafloor (Mudline), maps of top of salt, base of salt, and the zone of interest were prepared. Tiber Well in KC102 was loaded using the correct latitude, longitude, and depth (z) values. Once Tiber Well was positioned relative to the study area,

formation tops (base of salt, Upper Eocene, Cretaceous top and bottom) and well log data (Gamma ray, slowness, bulk density, etc.) were loaded into the Tiber Well input folder. Well log and mud-log data from BSEE were then correlated to the seismic data for quality, adding confidence to the well and seismic data by virtue of comparison. A 3-D view of the entire data

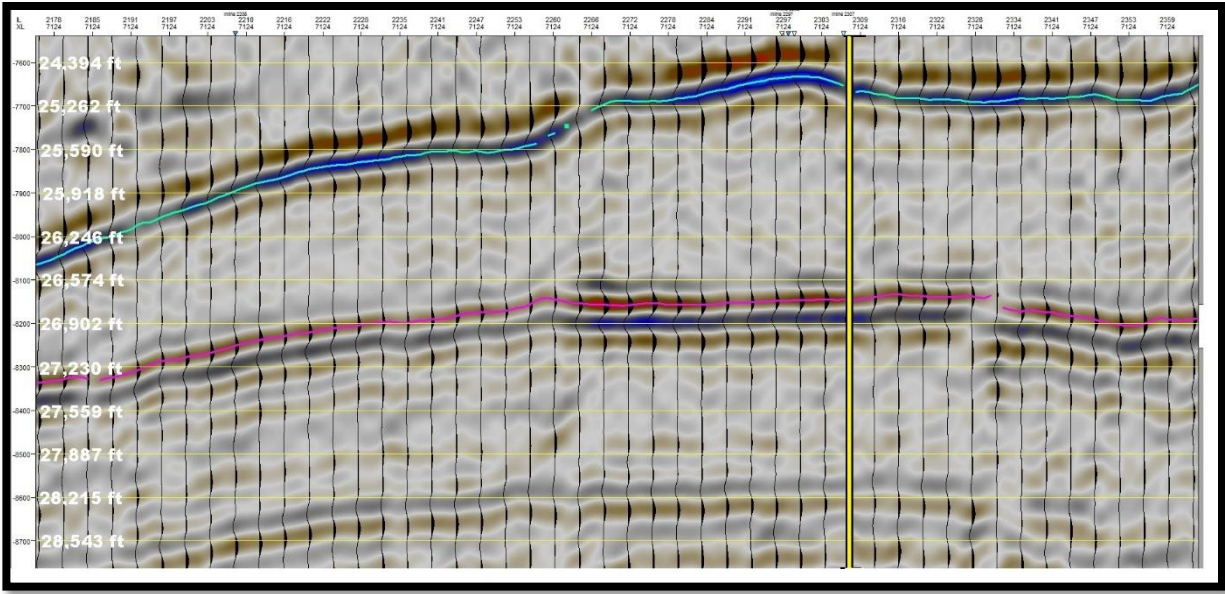


Figure 17. Dip parallel cross section of 2D seismic line with wiggle trace overlay. Figure created using Petrel 2013 E&P.

(figure 15) gives perspective to the immensity of the salt nappe dissecting the 16 blocks or 144 mi² of data. Figure 15 also indicates four notable horizons on a 2-D seismic cross-section (Base of salt, upper and lower surfaces of Subsalt Unit A, and the zone of interest), giving a relative proximity of the subsalt formations from base of salt at 24,980 ft to end of the Tiber Well KC102 at 35,055 ft. The zone of interest ranges from 24,000 ft to 27,000 ft, encompassing a range that extends above and below Unit A. The ZOI upper limit (24,000 ft) lies within the lower zone of salt approximately 1000 ft above the salt contact surface with Unit A and continues deeper through the base of Unit A and approximately 500 ft into the lithology below (27,000 ft).

The seismic investigation into Subsalt Unit A revealed an intriguing surface morphology. The ramp-like angled upper surface contains attributes that trend with the regional flow direction of salt in this area. Observations of Subsalt Unit A show an upper surface containing the evidence of sediment interaction with the migrating salt. In 2-D and 3-D representations of the upper

surface of Subsalt Unit A, a discernible, transport-parallel, package of lineaments are present. Using the seismic interpretation processes pane, the transport-parallel lineaments atop Unit A were measured on a 2-D seismic, strike-parallel, cross section highlighting the magnitude of the salt contact surface features (figures 13, & 24). Petrel measurement tools used for determining distances are directly correlated to the 'X' and 'Y' values within the CRS. These measurements give a better perspective to the extent of this system. As mentioned, the flat-and-ramp morphology is evident when viewing the upper surface from a dip parallel cross-section (figure 12). A wiggle trace overlay of the same 2-D dip parallel cross-section shows Subsalt Unit A with minimal stratified reflections between its top and bottom surfaces (figure 16).

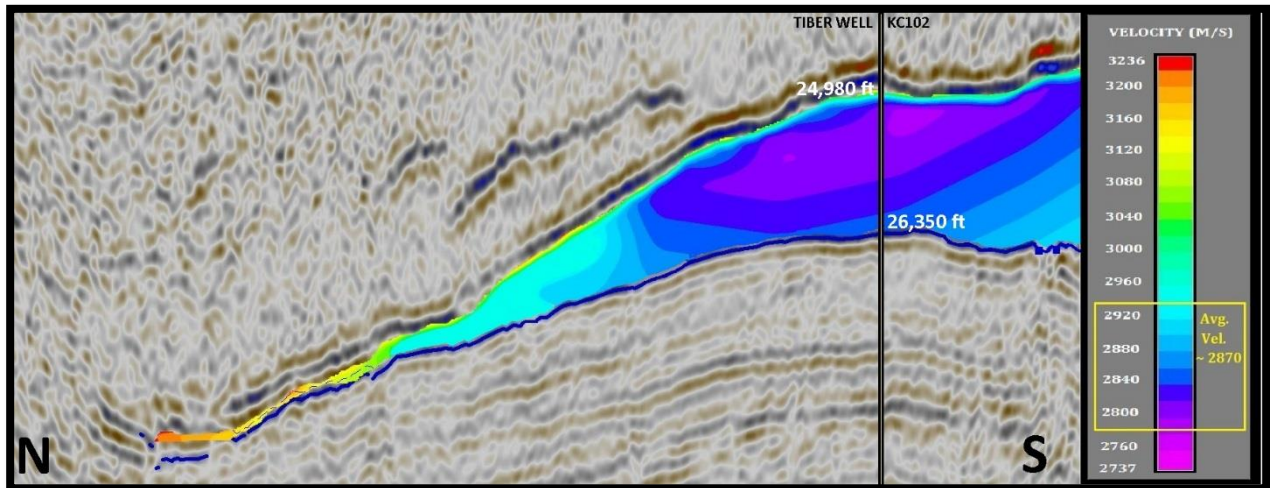


Figure 18. Dip-oriented 2D seismic cross section of Subsalt Unit A with cropped velocity model overlay. Figure created using Petrel E&P 2013.

The beam stack enhanced velocity model survey was used to create a cropped velocity model of Subsalt Unit A (figure 17). This approach allowed for the calculation of the quarter wavelength formula used to calculate vertical resolution. To establish vertical resolution, divide seismic wavelength by four (quarter wavelength formula: $\frac{\lambda}{4}$). Seismic wavelength is the result of

velocity divided by frequency, and the Nyquist and Dominant frequencies of the seismic wave are 100 Hz and 30 Hz respectively. Reflection coefficient is a good indicator of changes in lithology. Derived from a contrast in acoustic impedance between two materials, the reflection coefficient for a wave hitting a boundary or reflector at normal incidence (head-on) is expressed in equation 17. Comparing vertical resolution and reflection coefficient with gamma ray, porosity, and resistivity data, gives confirmation to the non-linear stratification seen on 2-D seismic lines within Unit A. This lack of stratification results from diapiric interactions with underlying sedimentary layers. When coupled with a possibility for fluid migration disrupting the stratified organization, zones like this are a critical point of focus when planning drilling operations through the base of large salt bodies.

In chapter 2, a petrophysical investigation within the zone of interest was performed utilizing published well log and mud-log data. Well data was collected, tabled, and processed using Microsoft Excel. Excel graphs compared depth to a number of variables, including temperature (degrees Fahrenheit while drilling), drilling mud-weights (psi/ft), bulk density (g/cm^3), pore pressure (psi), lithostatic pressure gradient (psi), overburden pressure (psi), fracture gradients (psi), shear and compressional wave slowness (converted to velocity in ft/s), caliper measurement, bit size, and casing size (in), reflection coefficients (unitless), seismic vertical resolution (ft, m), and acoustic impedance (ohm). These collected and processed data highlight the advantages of accurate pre-drill calculations on subsalt environments and provide insight into pre-drill investigations for similar operations in the future.

Chapter 2 is designed to identify the constitution of Subsalt Unit A, while providing a characterization of the potential hazards faced by drilling operations penetrating the base of

large salt bodies. The importance of pre-drill investigations when drilling in an environment such as this is due in part to abnormal formation pressures, which are often found in subsalt units in contact with the base of large salt bodies and within dirty salt. Great emphasis is placed on managing drilling fluid pressures in an attempt to avoid a pressure kick. A kick is a flow of formation fluids into the wellbore during drilling operations. A kick is initiated when pressure in the wellbore is less than that of the formation fluids, causing flow. If the mud-weight is too low, then the hydrostatic pressure exerted on the formation by the fluid column may be insufficient to hold back the formation fluid. The fracture gradient is the pressure required to induce fractures in rock at a given depth. Excessive mud-weight or hydrostatic pressure will cause the underlying lithology to fracture. These situations can occur if the mud density is not to specification or if a drilled formation has a higher pressure or lower fracture gradients than anticipated in the pre-drill investigations. Kicks caused by mismanagement of fluids, inaccurate calculations or predictions of in situ formation pressures, and lithostatic resistance to pressure, are commonly referred to as underbalanced kicks.

CHAPTER 1 – SEISMIC STUDY
INTRODUCTION

Near surface salt interactions with unconsolidated sediments have recorded a transport-parallel package of lineaments and a flat and ramp morphology. Such features are not typical of the base of allochthonous salt and this study happens to cover the type area (personal communication, Hudec, 2016). A combination of seismic interpretation and petrophysical

analyses focus on weak sediments at the time of shallow and passive emplacement as contributing factors to the morphology of Subsalt Unit A.

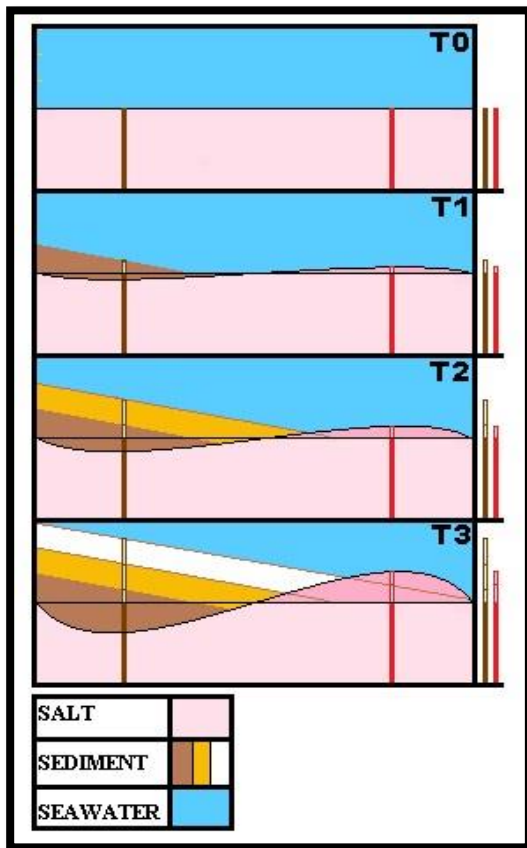


Figure 19. Gravitational instability with sediment/salt interaction (conceptual). T₀–T₃ relative time datum. Red and Brown bars on the right margin (also high and low points of curve) indicate the amount of uplift (red) or accretion (brown) over time. By T₃, there is a substantial amount of higher density material (sediments) overlaying the lower density salt.

SALT TECTONICS

Salt tectonics on passive margins like the northern Gulf of Mexico result from gravity instabilities initiated by the combined effects of basinward salt migration and sediment loading. A gravitational instability could be thought of as a viscous layer of low-density evaporites (halite) overlain by higher density sedimentary deposits (figure 18). The instability increases over time as

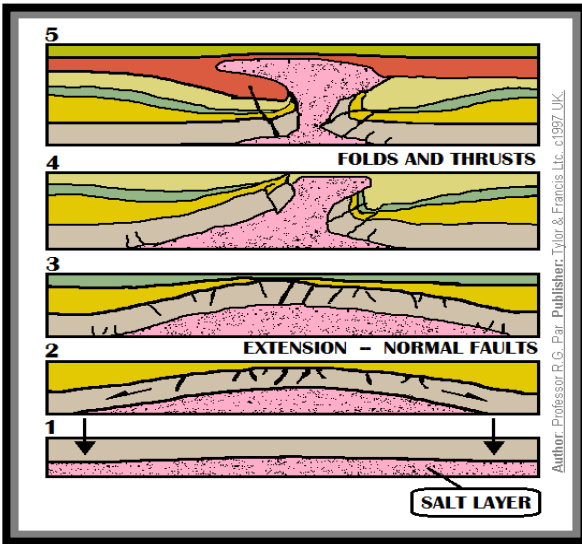


Figure 110. Evolution of a salt diapir. Sequentially numbered to represent deformation over relative time. Time datum are numbered 1 through 5 with 5 being the most recent of the examples. Pink is salt; grey, gold, green, and tan are sedimentary layers. Figure modified from Professor R.G. Par's publication in UK (1994).

accommodation space is created so the advancing salt commonly forms domes and other salt structures that invade nearby lithology (figure 19).

Substantial deformation by linked proximal extension, mobilization, and distal contraction are the result of salt gravity spreading and gliding (Diegel et al., 1995; Peel et al., 1995; Rowan et al., 2004). Three models have been proposed to explain how horizontal salt layers may evolve into diapirs. First, when

a sedimentary basin is stretched, reactive diapirs can rise, creating sharp ridges below strata, which thins by extensional faulting. Then, active diapirs can break through arch-like folds with crests that have been thinned by erosion. Finally, passive diapirs can grow like islands of exposed salt while the base of the diapir and surrounding sediments sink by gaining density as the sedimentary basin fills and sediments compact relative to salt. Reactive diapirism (Vendeville and Jackson, 1992a) is unlike the other two modes in that it requires regional extension (figure 20A). Above the salt layer, a normal syn-depositional or syn-sedimentary extensional fault releases, creating accommodation space. Also known as growth faults, extensional syn-faults initiate and evolve at the margins of continental plates extending parallel to passive margins with a high sediment supply (Cazes C.A., 2004; Schlische, R.W., and Anders, M.H., 1996). Salt flows easily into low-pressure areas, and when shallow enough, it does so by gravity spreading or

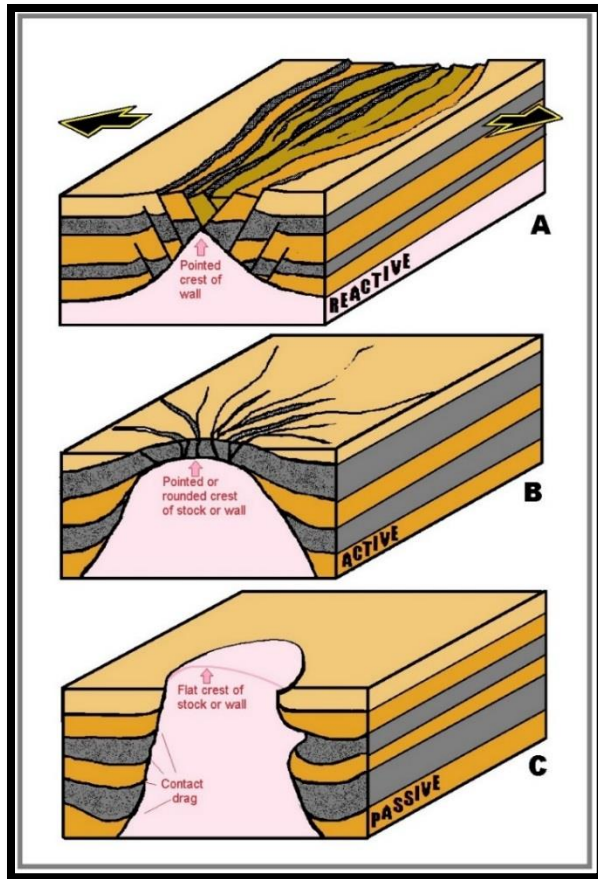


Figure 11. The evolution of diapiric piercement. From top to bottom, Reactive (A), Active (B), and Passive (C) modes of piercement. Schematic modified from Jackson et al. (1994).

gliding (figures 19 & 20). Active piercement (Nelson, 1991) describes a diapir forcefully intruding the overlying strata (figure 20B). Whether the salt follows the path of least resistance up the footwall of a fault or differential sediment loading causes salt to rise through weaker overburden, the active phase will eventually advance to a passive phase. A passive diapir (Nelson, 1991; Jackson and Talbot, 1991) remains at or near the surface while sediments accumulate discordantly around it, or erode away to reveal the present salt dome (figure 20c).

Sedimentary or structural truncation of

underlying strata against the lower contact of a salt tongue forms a basal cutoff with each cutoff, marking the former leading edge of the advancing salt tongue (Jackson et al., 1994). This is the result of a diapir in a phase of forceful, active piercement. Passive piercement consists of a ductile, viscous substance that when under substantial loading pressure, can infiltrate and displace the surrounding sedimentary units. In passive phase, the leading edge of a spreading salt sheet does not advance uniformly; alternatively, while the inflated salt dome spreads, it migrates along isobars of density, oversteps high-density materials, and infiltrates the weaker zones in the surrounding strata.

A salt gravity flow can potentially encounter resistant lithology capable of interrupting the advance. These obstructions cause the salt to diverge, circumnavigating the obstacle, and then converging on the other side. This happens in a manner similar to the way water in a stream bypasses a boulder and reconnects on the other side. The sediments in the streambed reflect the path of water around the boulder the way Subsalt Unit A

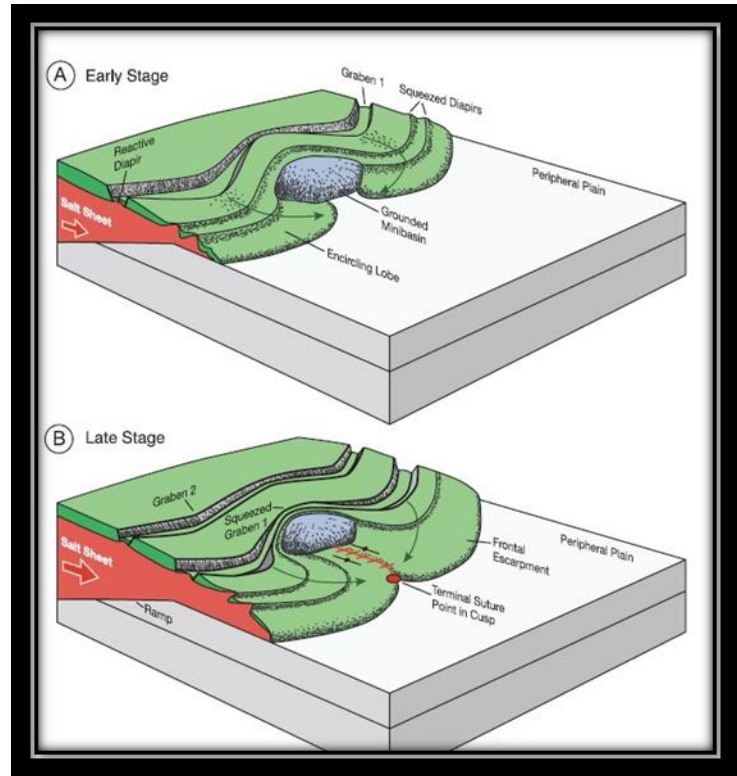


Figure 21. Dooley et al., (2012) showing how salt splits to avoid an obstacle and rejoins on the other side. Where the salt rejoins, sediment is collected and preserved as a suture.

reflects the bifurcation and rejoining of salt lobes. A coalescence of multiple lobes on the advancing salt sheet created the transport-parallel lineaments seen on Unit A. As lobes contact each other, sediments are formed into the ridge-like formations at the BOS contact surface.

CONCEPT

Whether single-feeder, salt separated and rejoined (Autosuture), or multi-feeder, converged with other sources (Allosuture), as salt lobes coalesce, they entrap sediment recording a suture. Autosutures can form when the salt overrides or encircles sediment and obstacles

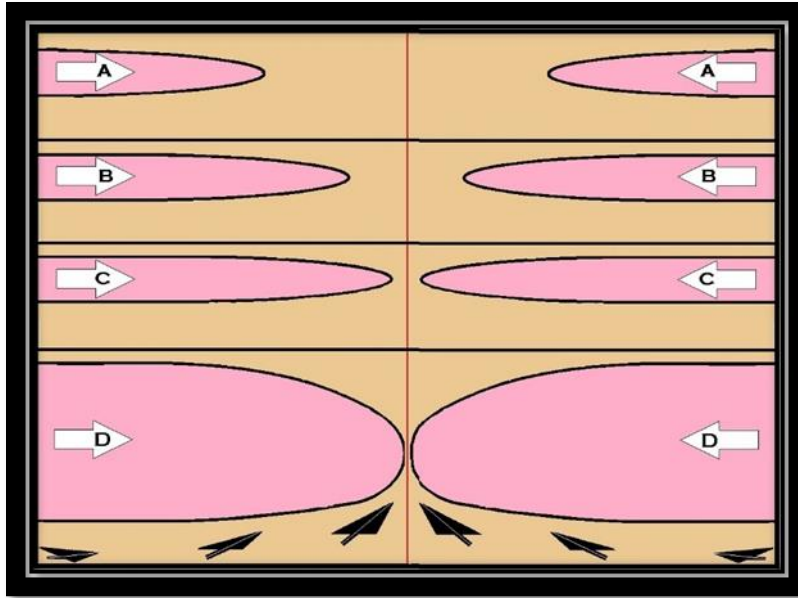


Figure 12. Conceptual schematic illustrating how the leading edges of salt lobes converge and collect sediment. A – D shows salt lobes approaching, D - illustrates the moment of contact between two converging bodies and the resulting suture ridge. Pink=salt, Brown=sediments.

(Dooley et al., 2012). An overriding autosuture is produced when part of a sheet overrides its neighboring sheet in the direction of salt emplacement. The overriding sheet subsides into the overridden sheet and traps sediments that can appear as intrasalt reflections. When encircling autosutures form,

two lobes of a sheet separate to bypass an obstacle and then rejoin on the downstream side (figures 21 & 22). The salt encircles obstacles and surrounding sediments leaving behind sutures that tend to be short and parallel to the dominant flow direction of salt (Dooley et al., 2012). These points of convergence have been called cell boundaries, seams, collision zones, sutures, and others, but all of these terms indicate a scenario where salt comes together. Currently, the term *salt-sheet suture* is generally accepted when describing the convergence of salt lobes. (Dooley et al., 2014) identifies sutures by how the sediments are fed and how they collide, in addition to the physical description of the suture. The Suture Terminology section in Dooley's manuscript was tabled for quick reference (table 5). The suture table illustrates the variability in sutures. In certain instances, the resulting suture formation consists of one or more sediment ridges, which are oriented in general alignment with the direction of salt emplacement.

CONCLUSIONS

Salt canopies, formed by the coalescence of salt sheets, are an integral part of the continental slope and deep-water areas of many passive margin salt basins (Dooley T.P. et al., 2011). Thin allochthonous salt sheets spread gravitationally over or through weak, sediments near the surface and have influenced the morphology of Subsalt Unit A. Seismic interpretation identifies notable morphological characteristics along the basal salt contact surface. These characteristics included a general ramp-like shape, flat and ramp geometry, and a transport-parallel package of lineaments. FR are the result of passive salt advance and piercement occurring at or near the surface. Unit A formed during a time when salt advance was characteristically changing mode of piercement from active to passive, and the upper contact surface morphology exemplifies the salt/sediment competition for accommodation space (figure 23).

A shallow and inflated diapir will undergo gravity-driven spreading that displaces and disarranges the sedimentary unit with which it interacts. In shallow depositional environments, newly deposited sediments have not had suitable time to compact and consolidate. These sediments do not resist the advance of salt with much vigor, setting the stage for emplacement and preservation. However, shallow and malleable sedimentary units are not ubiquitously compliant to the salt. The leading edge of salt can bypass or overtake the tighter and more resistant zones encountered while spreading. Migrating salt is limited by the surrounding stratigraphy. For instance, salt of density (x) will not flow through sediments of density (2x) without fault and fracture pathways. Thus, the leading edge of salt can be arcuate in form but it may not be uniformly arcuate due to its propensity to conform to resistant lithology as it flows.

A previous study of this subsalt unit identifies it as a Cenozoic sedimentary formation (Malbrough, 2015). Malbrough interpreted the TPL as resulting from glacial-like abrasions of the underlying sediments by the invading salt. The glacial phenomenon creating the morphology that Malbrough compares with Subsalt Unit A is called plucking or quarrying, which is a positive feedback, erosional process that collects and transports bedrock clasts called joint-blocks. The base of glaciers contain meltwater channels capable of transporting sediment and debris down dip. Glacial meltwater erodes the bedrock upon which the glacier rides by infiltrating stress cracks and fractures in the bedrock. When this meltwater refreezes, it expands the cracks separating the clasts from their parent formation. A cyclic freeze/thaw process (frost wedging or hydraulic wedging) continually expands the cracks and fractures eventually liberating the clasts as joint-blocks. Continued collection and transport of joint-blocks has potential to scar the bedrock creating transport-parallel: moraines, levees, and gouges or scars.

To accomplish gouges and scarring of the scale seen in Subsalt Unit A, the rafted sediment blocks must become 'plucked' by the salt and implemented for gouging valleys ranging 2 to 5 mi wide and up to $\frac{1}{3}$ mi deep. This task includes being able to withstand the extremely destructive forces associated with infiltrating and gouging the surrounding stratigraphy. Successfully gouging immature formations with rafted blocks of sediment would require that the rafted blocks retain enough mass through the late active-to-early passive diapiric phase-shift to remain effective as 'gouges'. Rafted sediment blocks are common in similar environments but rafted sediment blocks of immature and unconsolidated material could not effectively retain enough mass to gouge massive valleys. Viscous liquids have the ability to shear, and the flow regime of the advancing salt will laminate. The extreme bottom salt layers will move more slowly relative to

the more centralized salt due to forces of friction. As new, incoming salt moves in, it retakes the rafted sediment blocks. This process will continue removing the sediment block from contact with its parent sedimentary layer beneath, disabling it as a scouring or gouging agent. Basal scouring and gouging of subsalt sedimentary units is possible but the semi-disintegrated raft would not be able to gouge valleys as expansive as the TPL interpreted here.

The gross scale flat-and-ramp geometry at the contact with the base of salt (figure 12) is a consequence of an extrusive advance of allochthonous salt in a shallow environment, indicating how the salt formation is a result of normal sedimentary processes (Jackson et al. 1994). Directly

related to a passive phase of diapiric advance, salt ramps and flats are the steeply inclined and gently inclined, stair-step like segments seen in the base of a passively advancing salt lobe.

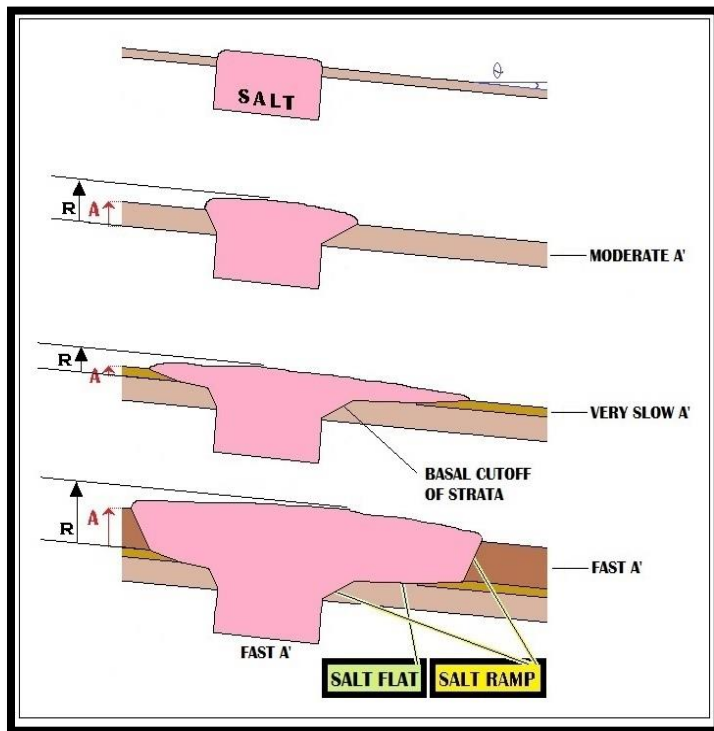


Figure 13. Asymmetric spreading of a salt sheet over or just below the sedimentary surface during the passive phase of diapiric piercement. Variable aggradation rates are evident in ramps, flats, and basal cutoffs along the base of the salt allochthon. A = aggradation increment, A' = aggradation rate. R = salt rise increment, Figure modified from figure 10 in Jackson, Vendeville, and Schultz-Ela (1994).

SUTURE TERMINOLOGY

A		CONFLUENCE
1	SUTURE	The zone separating two coalesced salt sheets (allosuture) or two lobes of a single salt sheet (autosuture), including trapped sediments.
2	SUTURE SURFACE	The surface separating two allochthonous salt bodies and their respective sediments. The salt bodies may be derived from different feeders (allosuture) or from a single feeder (autosuture)
B		SALT-FEEDER CONTRIBUTION
1	<i>AUTOSUTURE</i>	A suture between two lobes of the same sheet (single feeder).
2	ALLOSUTURE	A suture between salt sheets having separate feeders.
C		ORIENTATION of CONFLUENCE
1	FRONTAL SUTURE	Suture map trace is roughly perpendicular to the main direction of salt flow.
2	<i>LATERAL SUTURE</i>	Suture map trace is roughly parallel to the main direction of salt flow.
3	OBLIQUE SUTURE	Suture map trace is oblique to the main direction of salt flow.
D		LINE of ABUTMENT
1	SUTURE LINE	The trace of a suture surface on the plane of observation.
2	<i>BASAL SUTURE LINE</i>	Intersection of a suture surface with the base of salt.
3	APICAL SUTURE LINE	Intersection of a suture surface with the top of salt.
4	COMPOSITE SUTURE LINE	Intersection of three suture surfaces at a salt-sheet triple junction.
E		CONFLUENCE POINT TYPES
1	SUTURE POINT	End of a suture line.
2	<i>BASAL SUTURE POINT</i>	Intersection of a suture line with the base of salt.
3	APICAL SUTURE POINT	Intersection of a suture line with the top of salt.
4	TERMINAL SUTURE POINT	End of a suture line in map view.
5	COMPOSITE SUTURE POINT	Intersection of a composite suture line with the plane of observation.

Table 5. List of terms with brief descriptions for the identification of sutures. Table created from suture terms in Dooley et al., (2012).

Typically, flat and ramp morphology cuts up the stratigraphic section in the direction of emplacement. In Structural Dynamics of Salt Systems, Jackson et al., (1994) illustrate ramps as resulting from high rates of sediment deposition to low rates of salt advance, and flats as resulting from low rates of sediment deposition to high rates of salt advance (figure 23). Subsalt Unit A is positioned such that it appears to have formed during the transference from active to passive phases of diapiric piercement. As the shallow diapir began to spread laterally (gravity flow), salt

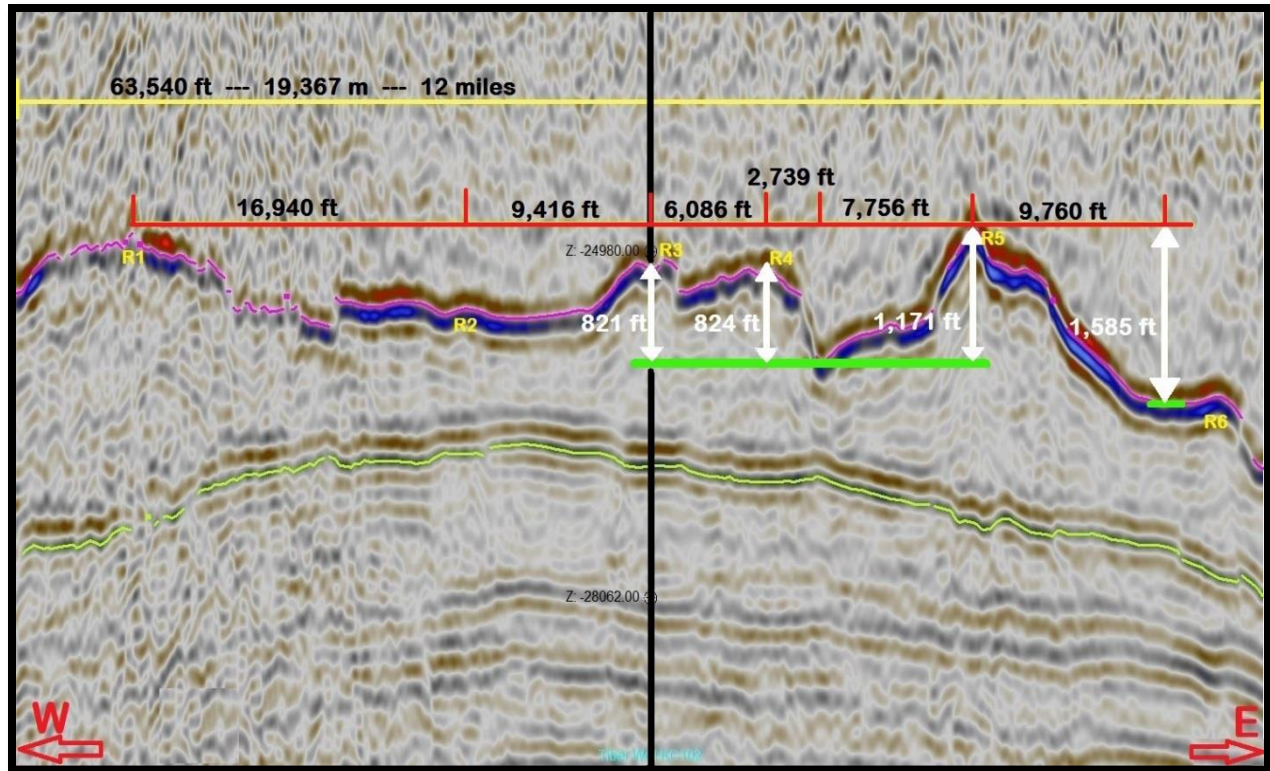


Figure 14. Transport-parallel lineaments with dimensions labeled in feet. Horizontal dimensions are red with black text. Vertical dimensions are white with white text. Black vertical line is Tiber Well KC102. Ridges are numbered R₁ through R₆ in yellow. Figure created using Petrel 2013 E&P.

and sediment competed for accommodation space. The approximate 30° ramp angle is dip-aligned following the generally inferred direction of salt migration in this region and represents a low-order function of the near surface environment of emplacement and deposition. The FR geometry is the higher order sibling-function of the general ramp geometry. Molded in a competitive depositional environment, the FR and general ramp geometries result from shallow, diapiric salt advancing into a zone of immature sediment while contending with an influx of new sediment for available accommodation space. The low order general ramp shape shows the rate of salt advance over time outpacing sediment aggradation, and the higher order FR geometry illustrate the cyclic nature of the emplacement-to-deposition ratios.

The transport-parallel package of lineaments (TPL) on Subsalt Unit A result from the advancing salt merging and mingling with sediment. The TPL align with the direction of salt emplacement and are observable on strike-oriented seismic cross-sections of Unit A. A complex series of high, steep ridges and deep valleys (figures 13 & 24) labeled R₁ through R₆, V₁ through V₃, and V_A through V_E comprise the general silhouette of the TPL. The TPL results from a type of suturing. As separate lobes of salt coalesce, they each bring along an accretionary mass of sediments. Squeezed as they collide, the entrapped sediments between the leading edges of sub-arcuate lobes create a steep ridge at the suture line.

The TPL of Subsalt Unit A are sutures that formed as the salt began to flow outward from the inflated crown of the diapir. Sutures are zones of entrapped sediments resulting from shallow, passive phases of diapirism and developed during a phase shift in diapiric piercement. Resulting from sediment interaction with diapiric salt, the TPL are single-feeder contribution allosutures with a lateral orientation of confluence, resulting in sub-parallel packages of basal suture lines that align with the regional direction of salt emplacement.

After migrating up from the confining and high-density strata below, the inflated crown of the diapir released and began spreading. With a steady supply of salt from below, the newly formed crown began to spread and flow laterally in a sub-radial or sub-arcuate fashion. Once the active/passive phase shift had concluded, sub-radial spreading begins to integrate with the regional salt sheet and surrounding sediments and sutures form as a result.

CHAPTER 2 – PETROPHYSICAL ASSESSMENT INTRODUCTION

The petrophysical study addresses potential hazards resulting from drilling through and exiting the base of salt and into the underlying sedimentary formations. This assessment identifies the constitution of Subsalt Unit A, introduces dirty salt and clean salt formations, processes well log and seismic data, and discusses pore pressure estimations for safe drilling procedures. Understanding the constitution and morphology of Subsalt Unit A, its long term shared interaction with salt, and the manifestation of formation pressure within the zone of interest will aid in the safe design of future projects in similar geologic architecture.

2D seismic reflections of large rafted sediment blocks and numerous inclusions qualify the salt in this dataset as dirty (figure 25). Clean rock salt is without pore space and therefore does not contain the incompressible fluids necessary to transmit overburden pressures. When a drill bit tags an inclusion whose pore fluids are subject to the overburden stress, the resulting pressure is transmitted to the borehole and must be appropriately contained. The zone of interest for this study ranges from 24,000 ft to 27,000 ft and has encompassed material above and below Subsalt Unit A whose depth is 24,980 ft to 26,500 ft at Tiber Well (figure 26). Extending focus beyond the upper and lower boundaries of Subsalt Unit A displays the interaction between the base of salt and the formations upon which it is riding. The data contained within BSEE-provided well logs were processed and graphed with a goal of identifying pressure and fracture

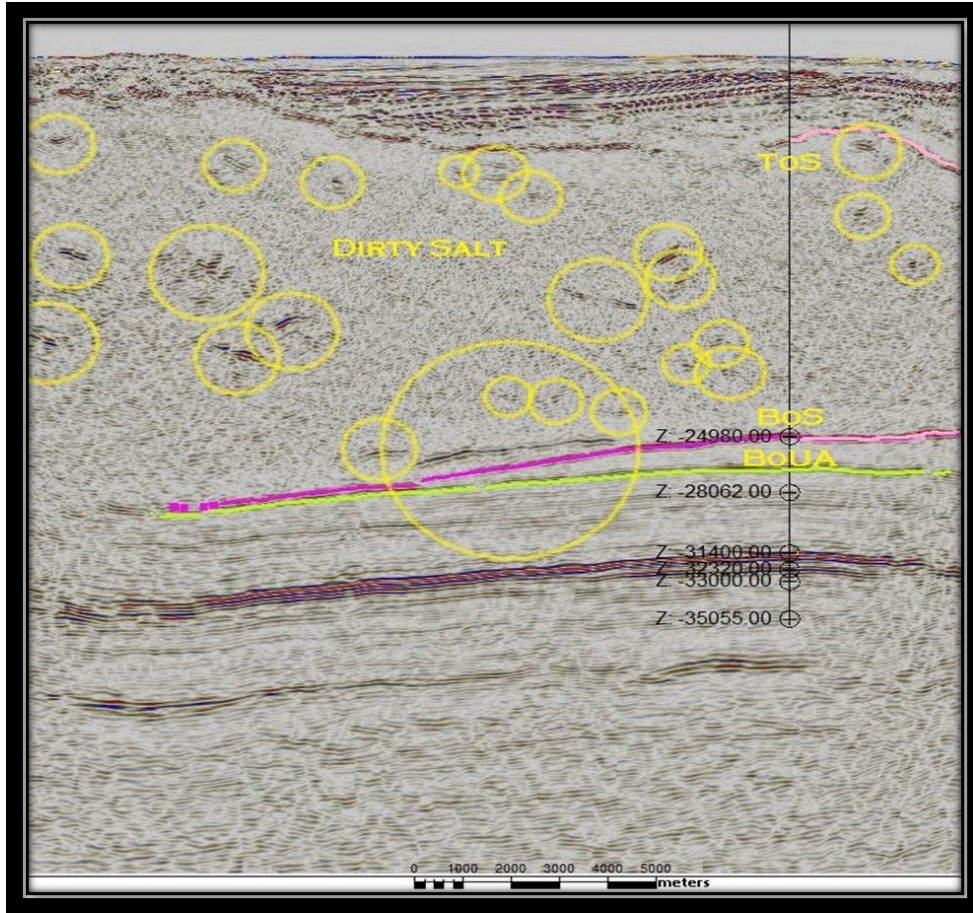


Figure 25. This dip-oriented 2-D seismic cross-section transecting entire dataset illustrates a dirty salt environment. Tiber well KC102 is the black vertical line, and formation top depths (ftMD) in black text. From top to bottom, the formation depths are; BOS, top of Wilcox, base of Wilcox, top of Cretaceous, base of Cretaceous, and total drilling depth. Yellow circles indicate rafted sediment inclusions within the salt. Figure created using Petrel E&P.

gradients within the zone of interest. Principal data include depth, mud-weight, lithology, density, temperature, acoustic logs, physical well condition, and tool string information.

WELL-LOG PROCESSING

Well depth measurements are referenced to a standard datum(s). Terms such as measured depth (MD), mudline/seafloor depth (ML), sea level (SL), drillers deck (DD), and Kelly bushing (KB)

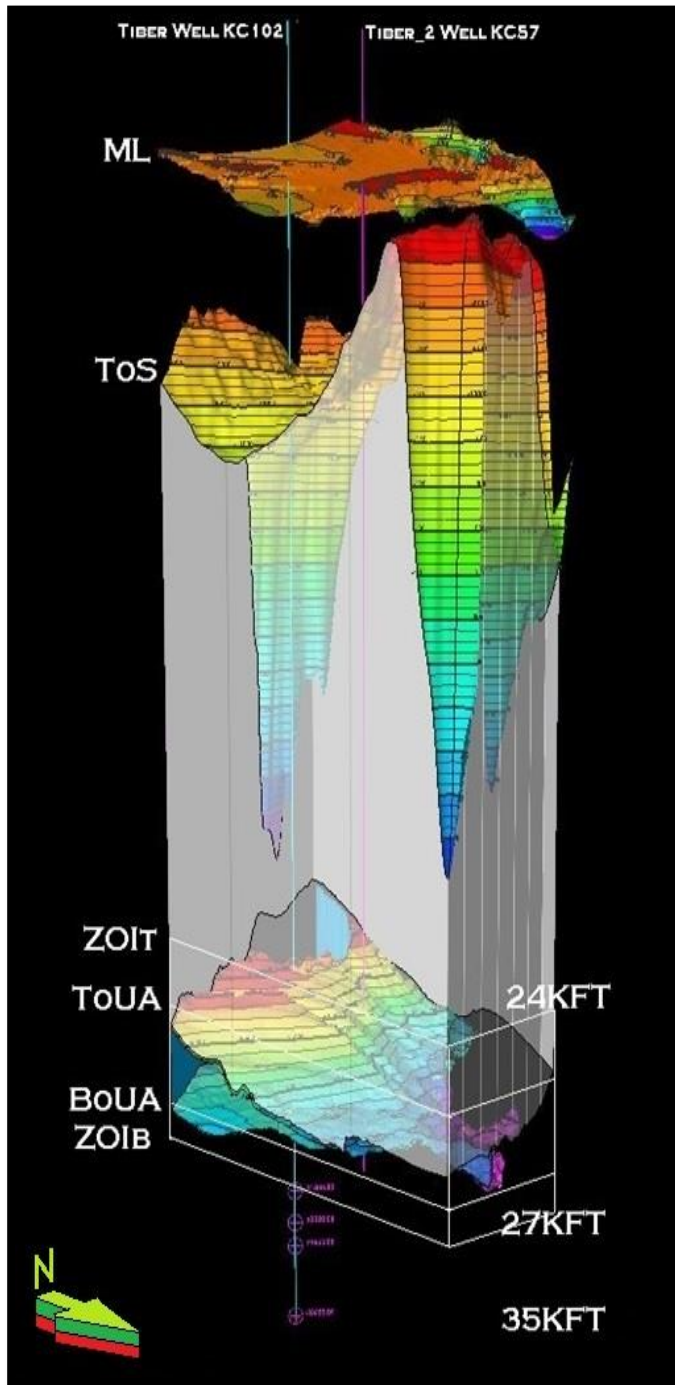
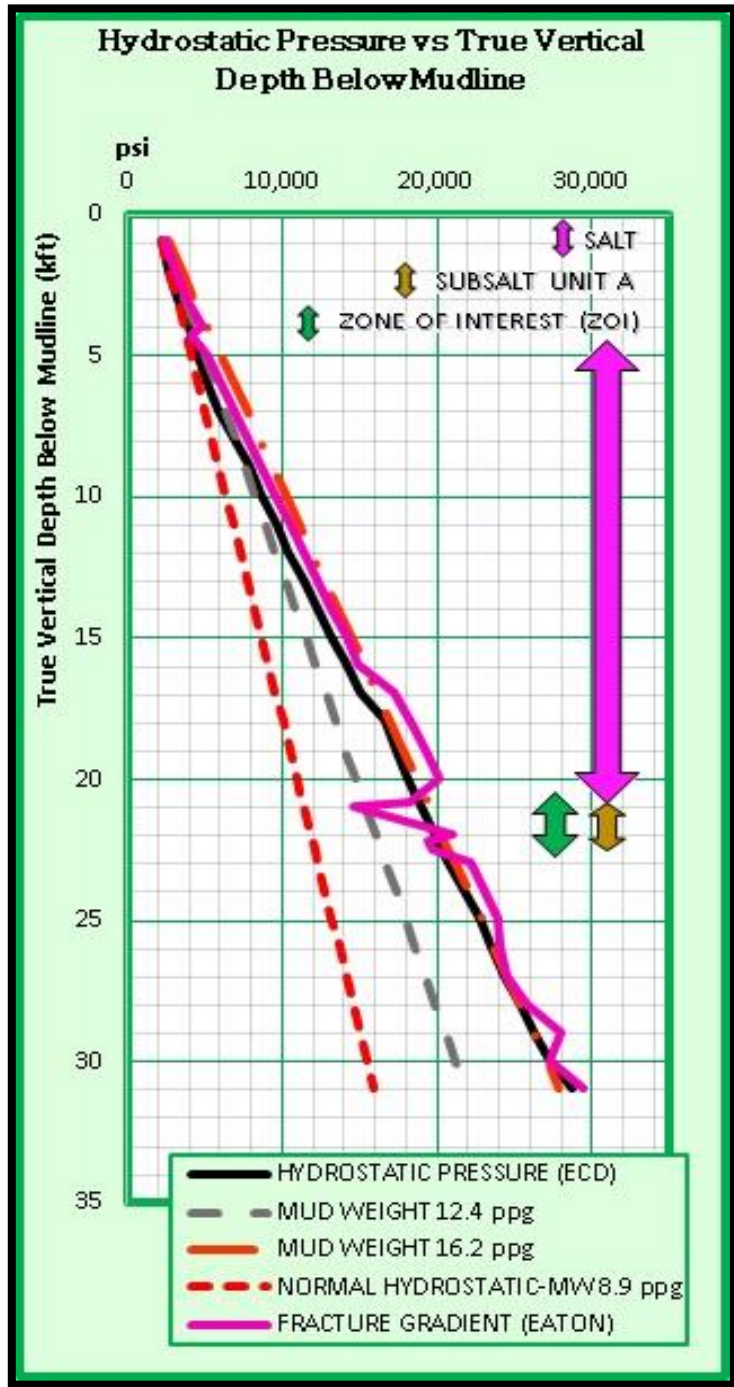


Figure 15. 3D model of data to a depth of 27,000 ft. ZOI = Zone of Interest. ZOIT = Top of ZOI. ZOIB = Base of ZOI. TOUA = Top of Unit A. BOUA = Base of Unit A. .Depths are in ft MD from Tiber Well KC102. Figure created with Petrel 2013 E&P.

are references by which we establish measured depth and true vertical depth. Referencing depth to multiple datum can lead to contradictions, so it is crucial to establish and identify the reference datum(s) used. In Tiber Well, elevation datum references the drill floor (DF) and water depth (WD), with the DF at 75 ft above sea level and the WD at 4,132 ft. A total distance spanning vertically to the mudline (seafloor) would be 4,207 ft. Depth was referred to sea level, mudline, and drilling depth as appropriate in the performance of necessary calculations. Mud-weight is the mass per unit volume of a drilling fluid, and means the same as mud density. Weight units are reported in lb/gal (ppg), kg/m^3 or g/c^3 (specific gravity), and lb/ft^3 , while pressure units are in psi/ft , and psi/kft . The mud-

weight controls hydrostatic pressure in a wellbore and prevents unwanted flow of formation fluids into the well, which is dangerous and has the potential to become catastrophic. Mud plays many critical roles throughout the drilling operation including the support of open hole bores and casings, which provide the structural support necessary to prevent collapse. Graph 1 reflects the mud-weight used in Tiber Well with a range or 'mud-fan' that is bound by the upper and lower static mud-weights (graph 1). This graph also illustrates the hydrostatic pressure, fracture gradients, and the limits of the salt nappe, Subsalt Unit A, and the ZOI.

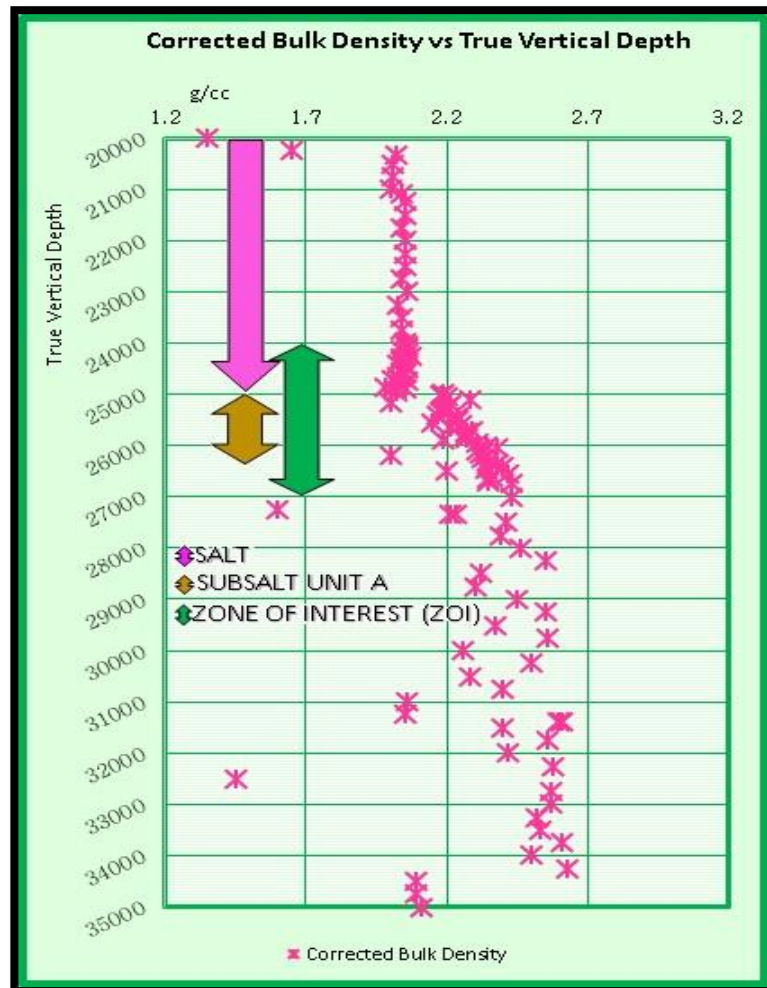
The Hostile Environment Litho-Density Sonde (HLDS) tool includes magnetic shielding and



Graph 1. Graph showing mud weight and hydrostatic information. Hydrostatic equivalent circulating density while drilling or (annular PWD ECD) is the thick black dataset. Mud weight (16.2 ppg) is red dash/dot dataset. Normal hydrostatic is red dashed dataset, and fracture gradient is in pink solid dataset. Note the downscale deflection in fracture gradient when passing through Base of Salt at approximately 21,000 ft. Graph created using MS Excel 2013.

high-speed electronics, deriving bulk density and photoelectric factors for drilling applications. The HLDS consists of a radioactive source with two detectors, which are pressed against the formation by hydraulically activated arms. The gamma rays emitted by the source experience two types of interaction, Compton scattering and photoelectric absorption. Compton scattering is an elastic collision by which energy transfers from the gamma ray to the electrons in the formation. This interaction forms the basis of the density measurement because the number of scattered gamma rays reaching the detector is directly proportional to the number of electrons

within the formation. Simply stated, the electron density of the rock is proportional to the bulk density of the rock. Corrected bulk density logs account for photoelectric absorption, which occurs when the gamma rays reach a low energy level after being repeatedly scattered by the electrons within the formation. A photoelectric effect index is determined by making count comparisons between the far detector and the short-spacing



Graph 2. Corrected bulk density vs. true vertical depth. Pink, brown, and green arrows indicate depth ranges of the salt body, subsalt unit A, and the zone of interest (respectively) within the graphed zone. Graph created using Excel 2013.

detector. The far detector is in the high-energy region where Compton scattering occurs, while the near detector, which is used to correct density measurements, is in the low-energy region where count rates depend on both scattering and absorption. Some useful applications for the corrected bulk density (graph 2) results are for porosity estimates, seismic impedance calculations, and rock chemistry definitions. With a known grain density, porosity is calculated

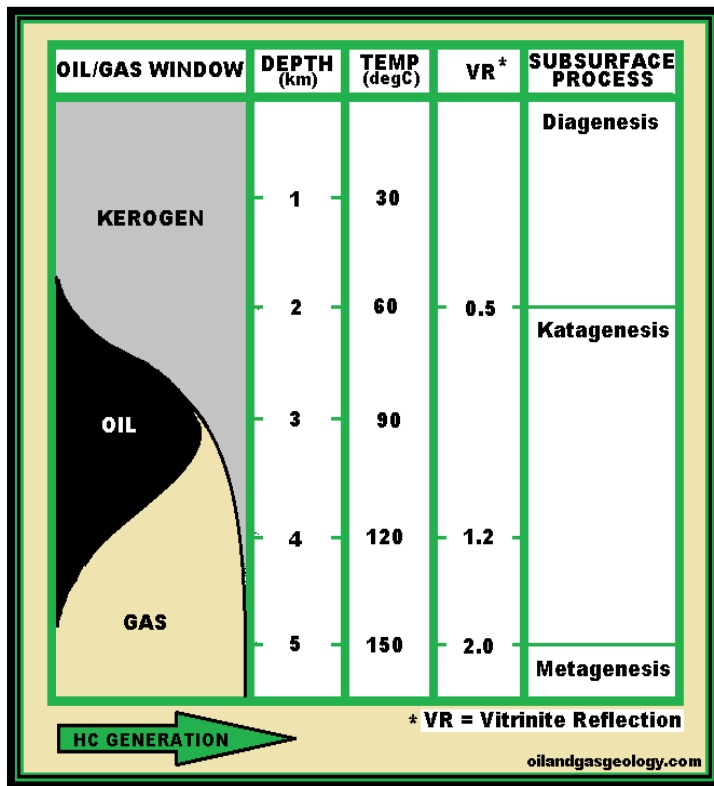


Figure 16. Generalized hydrocarbon maturity phase diagram from oilandgasgeology.com. Figure modified using MS Tools.

from the density log in the same way that porosity and density logs can be used equably for the calculation of grain density. The density log also contributes to the identification of lithology and lithologic boundaries. Each element is characterized by a different photoelectric factor that can be used alone or in conjunction with other logs when determining lithology type. When viewing density logs, the primary curves used for interpretation include bulk density

(RHOM in g/cm³), photoelectric effect (PEFL in barns/electron), density correction (DRH in g/cm³), and caliper (LCAL in inches). Primary log curves are typically displayed with the neutron curve (APLC) and with the assumption of constant grain density within the matrix, making a density porosity (DPHI) calculation possible.

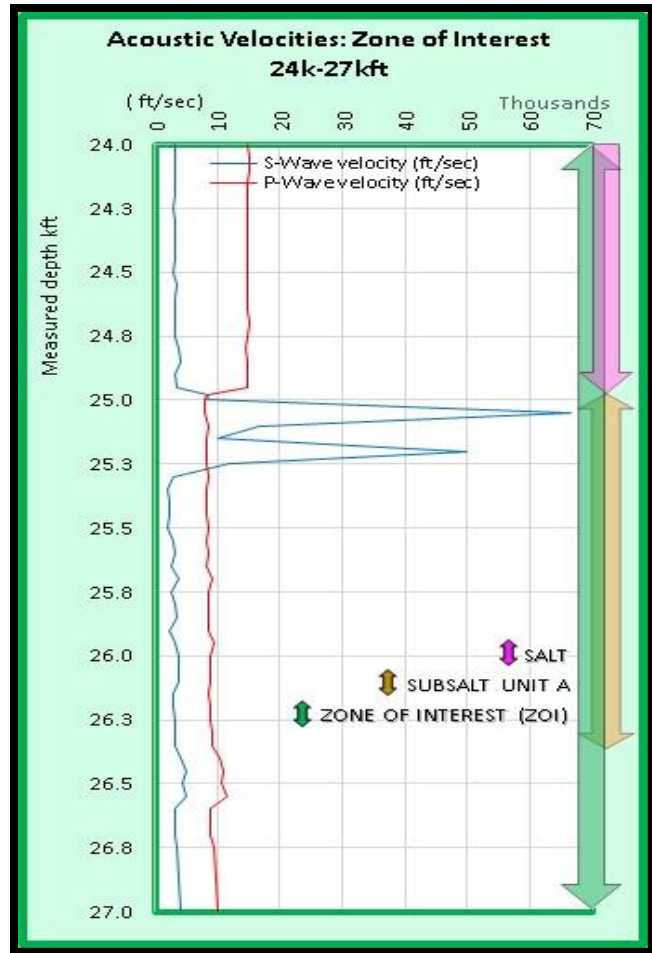
Subsurface temperatures and corresponding geothermal gradients influence drilling operations in at least three ways. Reservoir quality/diagenesis, source rock maturation, and potential for corrosive amounts of CO₂. Figure 27 illustrates the temperature dependence and phases of source rock maturation.

Acoustic logs measure the travel time or transit time for seismic waves per unit distance, (typically converted to microseconds per foot ($\mu s/ft$)).

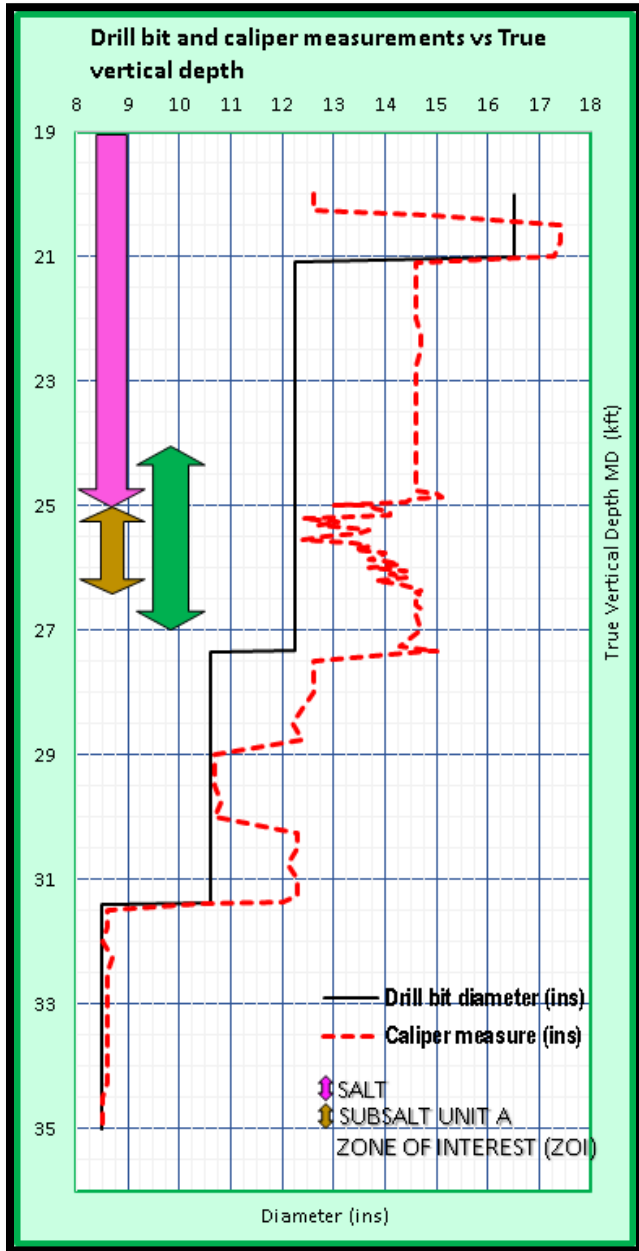
Compensated acoustic logs have two transmitters that are pulsed alternately. The measurements are then averaged to

cancel errors caused by sonde tilt or changes in hole size. Expressions relating velocity to porosity are used for inferring porosity from well logs. The equation: $\tau_\rho = \tau_s + \tau_F$, where τ_ρ is the measured travel time of a P-wave, τ_s is the expected travel time in the solid-phase material, and τ_F is the expected travel time in the pore fluid (Wyllie et al., 1956). This follows from $\frac{1}{V_\rho} = \frac{1-\phi}{V_{\rho^s}} +$

$\frac{\phi}{V_{\rho^F}}$ where F is porosity, V_ρ is the measured P-wave velocity, and V_{ρ^s} & V_{ρ^F} are the P-wave



Graph 3. Acoustic velocities for Zone of Interest. S-wave velocities are extremely high after penetrating base of salt as compared to P-wave velocities creating a zone of uncertainty. Graph created using MS Excel 2013.

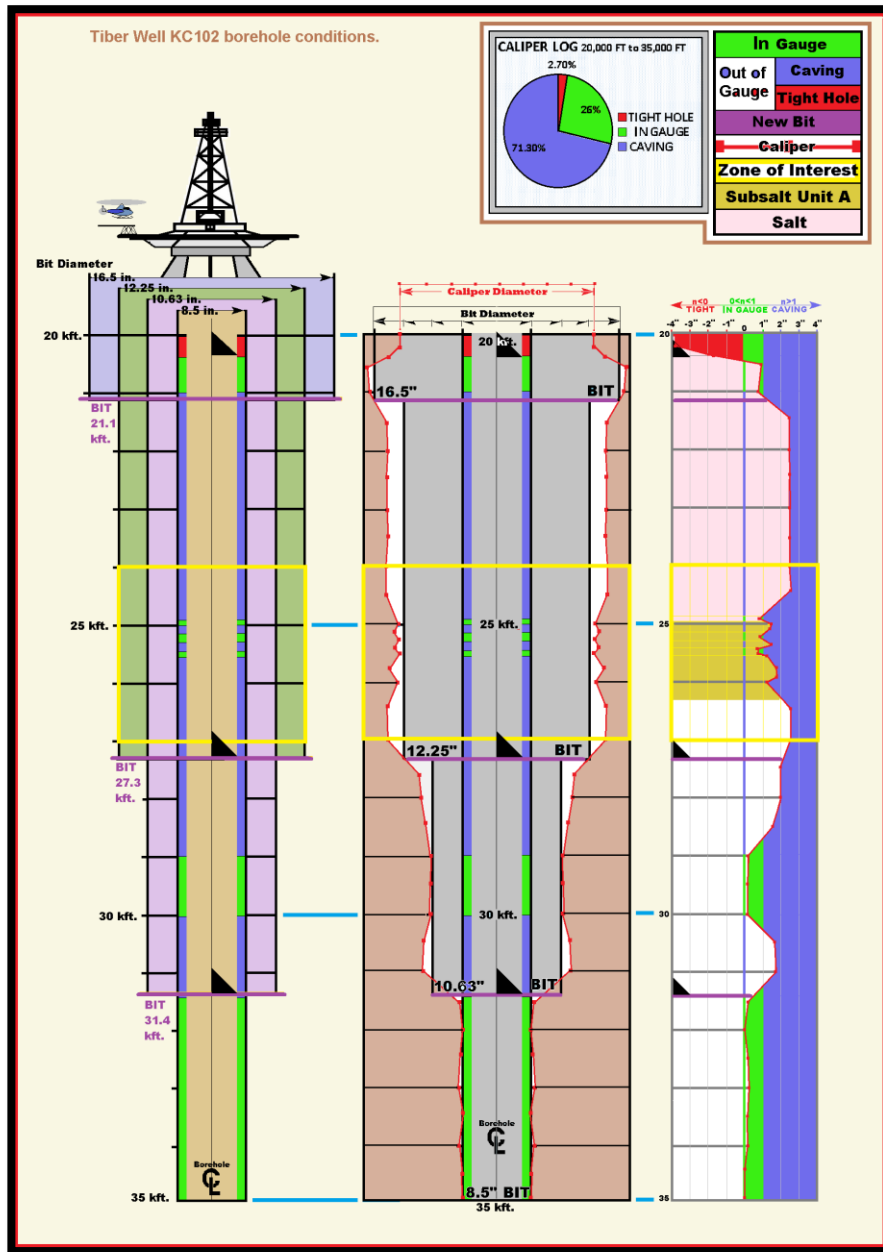


Graph 4. Comparison of caliper measures to drill bit diameter. This graph identifies borehole condition at a glance. Borehole condition is measured by comparing drill bit diameter (ins) to caliper measure (ins). The resultant deviation will classify the borehole as In gauge or Out of gauge. In gauge indicates very little bit diameter-to-caliper measure deviation. The out of gauge classification has two subsets; Tight hole (borehole diameter lesser than drill bit diameter), and Caving (borehole diameter greater than drill bit diameter).

velocities in the solid and pore fluid phases respectively. Acoustic logs from Tiber well are Delta-T compressional slowness and Delta-T shear slowness. Slowness (p) is the reciprocal of phase velocity and is related to the wave number (k) by $k = \omega p$ where (ω) is angular frequency. The wavenumber is the number of waves per unit distance perpendicular to a wavefront and is reciprocal to the wavelength. To validate the consistency of density and acoustic data, velocity was calculated using density with the bulk, shear, and compressional moduli in addition to taking the reciprocal of slowness ($p^{(-1)}$). The results were identical, giving validation to the corrected bulk density calculations.

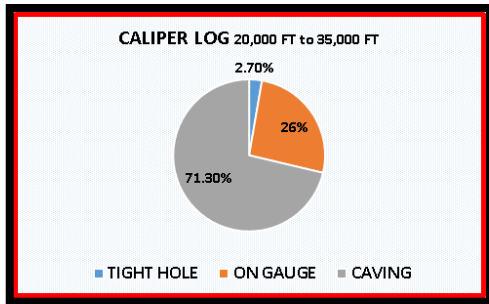
Graph 3 shows the P, and S-wave acoustic velocity profiles within the zone of interest.

The zone spanning 24,900 ft - 25,700 ft,



contains the result of acoustic log measurements that are out of log display range and/or near the range limits.

Caliper measures determine quality of all other log data. Caliper data generates a physical profile of the well (figure 28). The caliper log indicates the deviation between bit and borehole

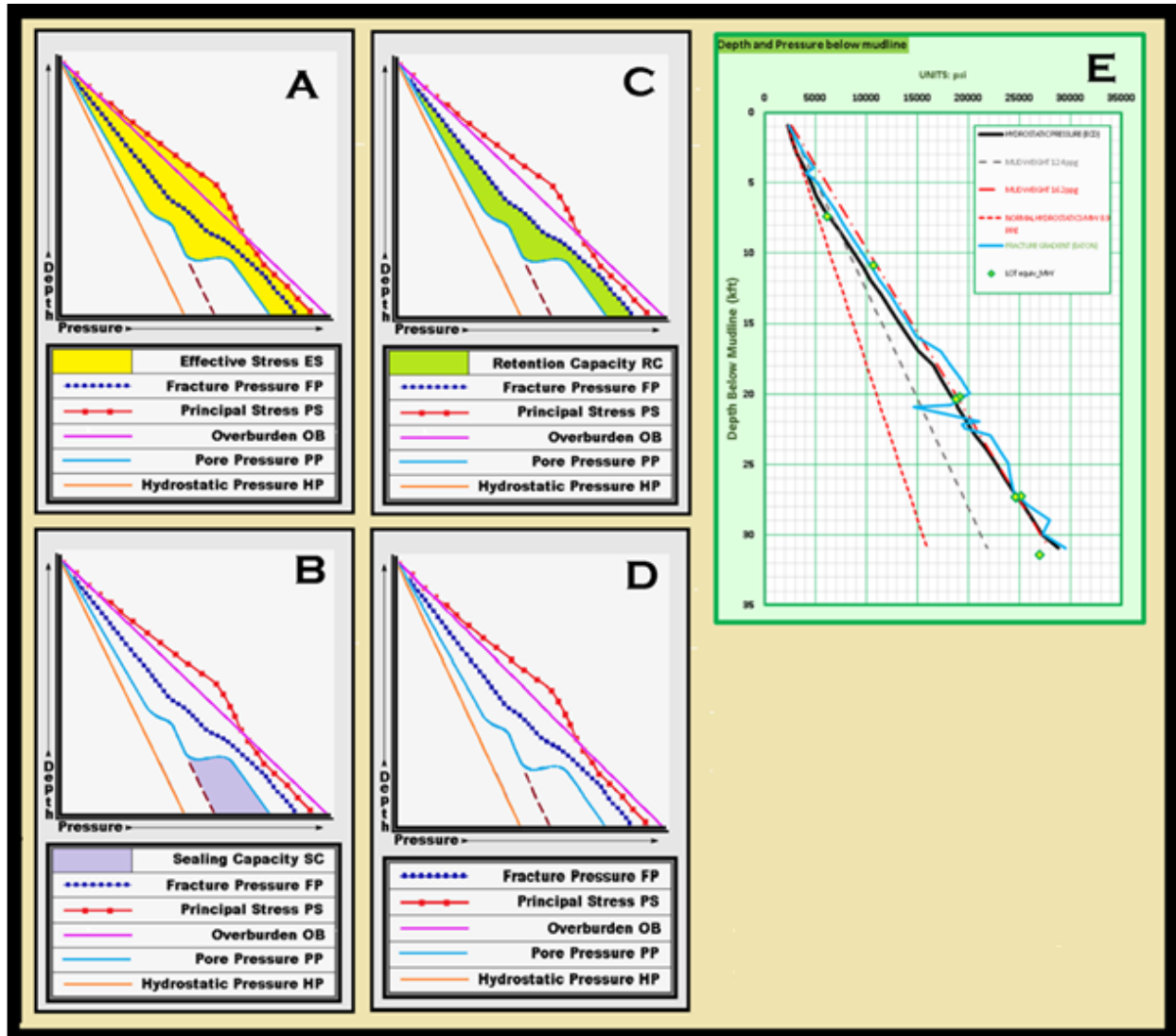


Graph 5. Borehole conditions at Tiber Well KC102 from 20 kft to 35 kft displayed as percentages of each condition. Graph created using MS Excel 2013.

diameter measures. The post-drill borehole profile is categorized as in gauge or out of gauge. For this study, in gauge is defined as $caliper - bit\ diameter = 0\ to\ 1\ in$. An out of gauge-caving scenario is defined as $caliper - bit\ diameter > 1\ in$, and an out of gauge-tight hole scenario is defined as $caliper - bit\ diameter < 0\ in$. Bit size and caliper measure at Tiber are shown in (figure

28 and graphs 4 & 5). The distribution of borehole condition for the 15,000 ft span is 71.3% caving, 26% in gauge, and 2.7% tight hole. Graph 4 compares bit size and caliper reading to true vertical depth. Any borehole diameter measurements beyond the in gauge range limits can potentially limit the quality and precision of various well log results. However, centralized tools are designed to operate within a specified tool-to-formation thickness, which is the distance from the center of the tool to the wall of the formation. If a borehole caves and increases the tool-to-formation distance, tool response and reliability can be degraded. In an out of gauge scenario, useable log data may still be obtained with the application of suitable correction factors. A suitable example of caliper-aided correction would be supplementing data for an HLDS that transfers radiation through hydraulically activated arms that remain pressed against the formation. Absorption factor is affected when the tool loses contact with formation, resulting in errors of measurement. In this example, the contributory properties of the caliper log would endorse correction factor estimations for bulk density.

Observing fluid pressure changes requires tailoring the mud to profile adequately within a prescribed pressure range. For safe and efficient operations, Annular PWD/ECD (Performed



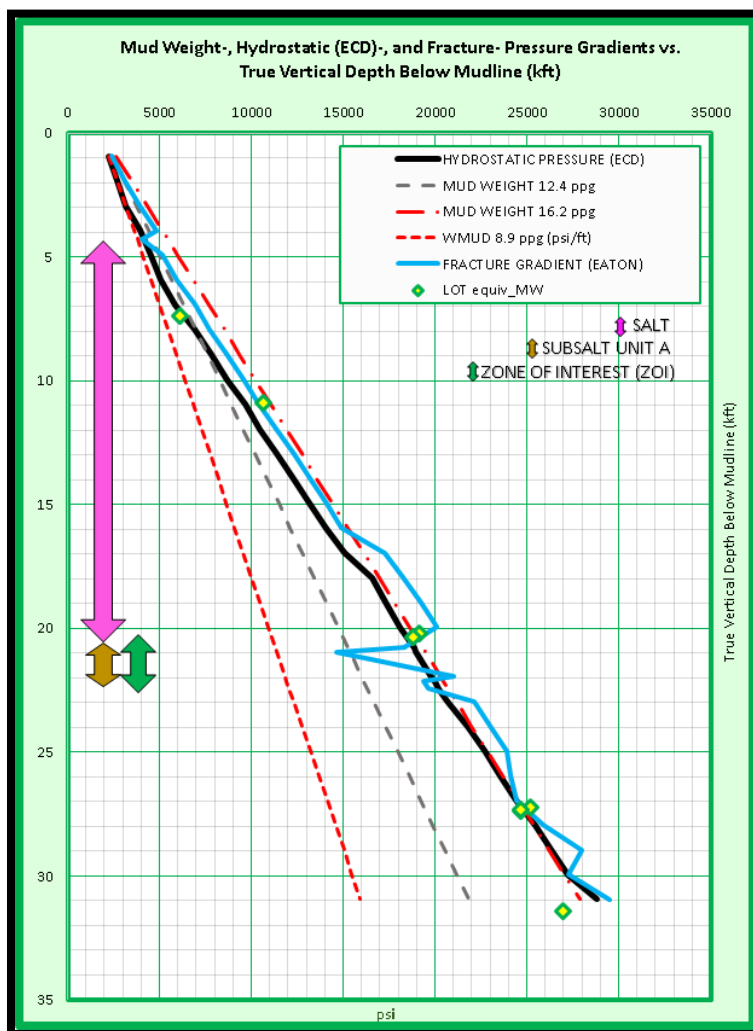
Graph 6. Depth versus pressure examples of subsalt sedimentary units, which illustrates; fracture pressure, effective stress, sealing capacities, and retention capacities. Shaker, (2015) graphs A – D, are compared to Tiber Well KC102 graph (E) to. Composite graph created using MS tools.

While Drilling/Equivalent Circulating Density), and static mud-weight, shall be regulated to remain within the prescribed drilling tolerance window (DTW) (graph 6). If mud-weight exceeds the upper limit of the DTW it has potential to fracture the formation resulting in a loss of circulation. A loss of circulation results from mud going into a formation rather than returning up through the annulus. This happens due to formation breakdown during drilling as well as in naturally fractured or cavernous formations. If mud pressure is less than that of the formation

pressure (below the DTW), fluids from the formation may escape into the borehole causing a kick. To avoid borehole stability issues, both ECD and static mud weight must remain between the pore pressure (PP) and fracture pressure (FP). Excessively increasing mud-weight (MW) in anticipation of overcoming a high fluid pressure environment can cause fracturing and loss of circulation (LOC) necessitating the addition of extra casing strings to the well design (Shaker, 2008).

SALT

Drilling through tabular salt adds elements of complexity to predicting subsurface pressures and designing mud programs. Two classifications are clean salt and dirty salt. Clean salt is essentially pure halite where dirty salt contains sediment inclusions, rafted sediment blocks and salt welds (figure 25).



Graph 7. Mud weight, Annular PWD ECD, and fracture pressure gradient, versus true vertical depth below mudline (kft). Pink, green, and brown arrows indicate Salt, ZOI, and Subsalt Unit A (respectively). Graph created using MS Excel 2013.

In some cases, a clean well path trajectory is possible in a dirty salt region. Noticeable deflections present in the gamma ray, resistivity, and porosity logs throughout the 16¹/₂ thousand foot Tiber Well salt transect correlate with inclusions seen in seismic views. Additionally, the mud-weight pressure gradient is high to contend with the formation pressures associated with salt inclusions. Well log data supports seismic data in locating the clean/dirty salt interfaces encountered along the well path.

Shaker, (2009) interprets salt overlying the Jack prospect (Walker Ridge Block 759; 125 mi SE of KC_102) as part of the Sigsbee salt toe. The Jack well penetrated sedimentary inclusions or rafts within salt, which exhibited fluid pressures higher than anticipated causing kicks and making this prospect very expensive to drill. The well underwent borehole stability issues including lost circulation events due to the narrow drilling window (graph 6). As a result, several bypasses and sidetracks drove production costs high. In contrast, Shaker mentions a case study in St. Malo located in Walker Ridge Block 678 (140 mi SE of KC_102) as an adjacent prospect on the same trend. When drilled, through a clean salt, St. Malo tested with a minimum of difficulties as compared to the Jack prospect.

WELL CONTROL

Pore pressure is the pressure on the fluids locked in the pore space of a formation. Where incompressible pore fluids support some of the overburden pressure, higher than “normal” (0.465 psi/ft) pore pressure gradients, also called geopressures, result. Although there is no such thing as an incompressible fluid, the term applied here considers a negligible change in density with pressure, which is usually the case with liquid.

The vertical distribution of pore pressures in the subsurface can generally be divided into four zones (from shallow to deep A, B, C and D respectively). Shaker, (2015) describes Zone A (shallow, free-flow) with pressure as a function of depth and a hydrostatic pressure gradient derived from the brine water column only. In the GOM, this gradient is approximately 0.465 psi/ft. Zone B (Hydrodynamic) starts at a depth where the OB stress begins the dewatering process. GOM pressure gradient in this zone ranges 0.52 psi/ft to 0.59 psi/ft. A stress model by Terzaghi and Peck, (1948) where $0.465 < \lambda < 1$ (λ is the ratio of pore stress to total OB stress) exhibits how velocity begins the exponential increase at the top with a reverse trend at the base.

Poisson’s ratio (ν , σ) is an elastic constant measuring the compressibility of material perpendicular to the applied stress. More commonly expressed as the ratio of latitudinal to longitudinal strain. ν can be expressed in terms of properties that are typically measured in the field, such as P-wave (V_p), and S-wave (V_s) velocities $\nu = \frac{(V_p - 2V_s)^2}{(V_p + V_s)^2}$. ν in the upper ZOI is relatively high from a depth of 20,000 ft to 25,000 ft, but otherwise has average values for the GOM Miocene. The high ν values (> 0.4) between 20,000 ft and 25,000 ft are in the salt. In salt, pore

pressure (PP) is negligible and Pr does not apply. However, expect to see variations in Pr results throughout a dirty body of salt like the one in this study. These high Pr readings may be due to the sediments having been buried and isolated before reaching compaction maturity. However, the Pr results are still high, which typically indicate very low tensile strength sediments. Poisson's ratio for carbonate rocks is ~ 0.3 , for sandstones ~ 0.2 , and greater than 0.3 for shale. The Poisson's ratio of coal is ~ 0.4 , Pr in hard material is very low, and Pr in pure water reaches 0.5. Average Pr for the GOM Miocene is approximately 0.3 (per. Communication; Jones, J., March 2016). An important note when using Pr is that if $V_s=0$, then Pr equals 0.5, indicating either a fluid (shear waves do not pass through fluids) or a material that can maintain constant volume regardless of stress, also known as an ideal incompressible material (Schlumberger Oilfield Glossary).

In dirty salt, encased sediments have led to the PP increase, and therefore drillers increase MW accordingly. Salt PP should have the same value from the point when the drill bit tags the TOS until it reaches the base of salt. PWD-EWR in Tiber Well at the upper and lower salt limits are 9.5 ppg and 14.4 ppg respectively, with a greater than 50% increase confirming the dirty salt observations. The mud-log notes salt inclusions of Red Clays and Anhydrites, indicating either a very shallow or a terrestrial environment of deposition. Seismic indicates numerous rafted blocks and inclusions within the salt body. Salt infiltrates the underlying sediment, creating a zone of rubble, or gouge zone, at the base of salt. Subsalt Unit A is a gouge zone. Evidence of this lies in some of the inherent features of Unit A. These features include a general lack of striated linear reflections, the TPL of the upper surface, formation pressures, and the observed petrophysical properties.

Newly drilled formations are pressure-tested below the casing shoe. Casing shoes have a round profile designed to guide the casing string past any impediments or protuberances that would otherwise prevent the string from being appropriately located inside the wellbore. After a casing shoe track has been drilled, the next step is a Formation Integrity Test (FIT). This is performed to determine the strength and integrity of a newly drilled formation by increasing Bottom Hole Pressure (BHP) to the designed pressure. The test is normally conducted to ensure the formation below the casing shoe will not be fractured while drilling the next section containing higher BHP, or to prevent circulating gas from causing a loss of well control. This test allows for accurate casing, cement, and formation evaluations that are very valuable to subsequent work in the well. The FIT helps to determine casing depths, well control options, and

DEPTH (md) BELOW ML	DEPTH (md)	FIT-STATIC MW (ppg)	FIT-TEST PRESS (kpsi)	FIT-TEST DENS (ppg)	FIT-EQIV MW (ppg)	LOT-STATIC MW (ppg)	LOT-TEST PRESS (kpsi)	LOT-TEST DENS (ppg)	LOT-EQIV MW (ppg)	NOTES
7.381	7381	10.22	0.465	10	11.2				11.2	
10.873	10873	15.8	2.152	11.8	15.6				15.6	
20.220	20220					15.47	1.45	15.1	16.47	* Pumped 16.75ppg to 10kpsi over against casing shoe.
20.343	20343					15.1	1.062	15.3	16.05	* Halliburton pumped 26.5 bbls bled back 10 bbls, open upper annular, pump up static density to 16.26-ppg.
20.356	20356		0.406							2 FAILED TESTS. * 406 down to 264 in 3 mins. * 405 down to 194 in 10 mins.
27.352	27352					15.59	1.062	15.3	16.05	
27.245	27245					15.3			16.48	
27.330	27330					15.3			16.05	
31.410	31410	15.73	2.142	15.4	16.71	15.73			15.4	* FIT test at 31410' press. 2142 down to 2046 in 10 mins.

Table 6. Formation integrity and Leak Off Tests. Information collected from the borehole profile description in the Mudlog report (BSEE). Table created using MS Excel 2013.

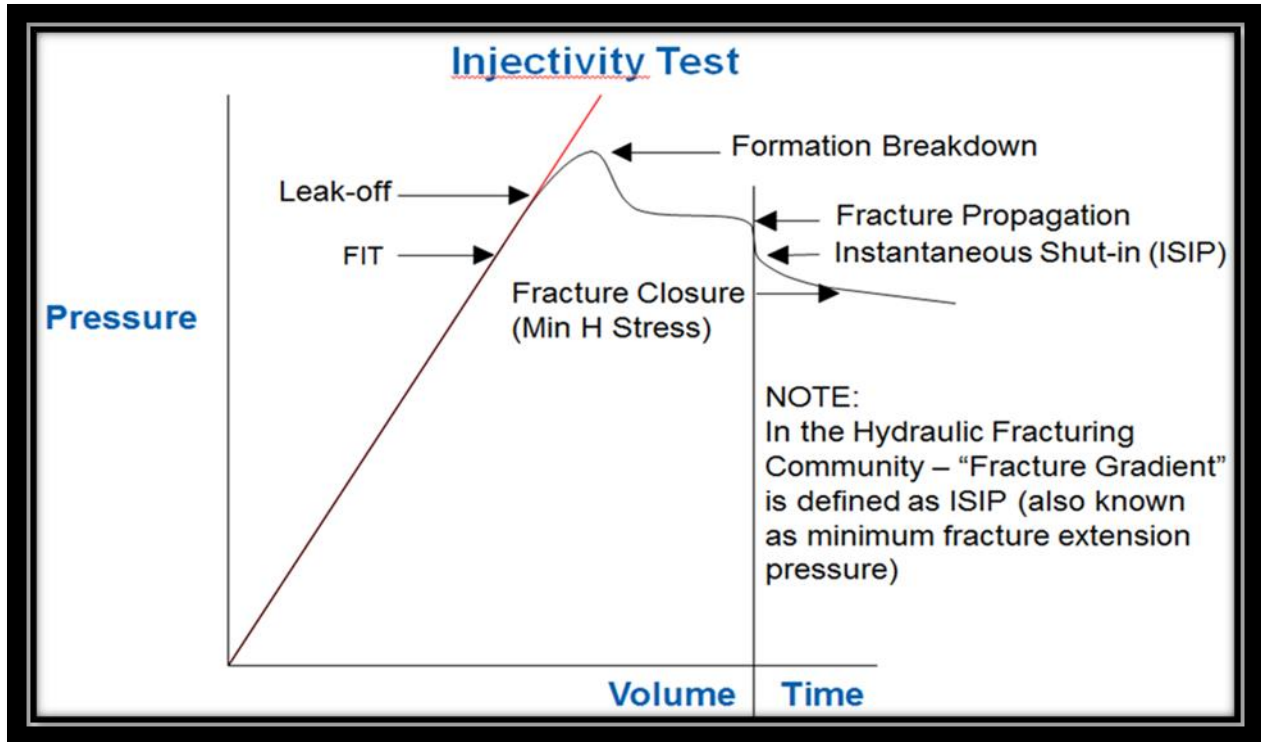


Figure 18. Classic example of an injectivity test. Diagram provided by John F. Jones Senior Staff Drilling Engineer, Marathon Oil - Worldwide Drilling and Completions.

the derivation of fracture pressures demonstrates how the calculation is performed; (Pressure required for FIT in psi) = ((Required FIT in ppg)- (Current Mud-weight in ppg)) * ((0.052) * (True Vertical Depth of the casing shoe). Leak off Tests (LOT) determine the fracture pressure or durability of the formation and are usually performed to test the installation of a new casing shoe (table 6). The pressure tests are applied to the formation directly below the shoe once it has been set and the drilling has resumed. It determines the safe maximum pressure that can be applied to the surrounding formation without breaking down. This information is an integral part of well control because it determines the mud program for the next formation to be drilled while helping to set safe limits on casing choke pressures. During the test, the well is shut-in and fluid is pumped into the wellbore to gradually increase the downhole pressure. At some point,

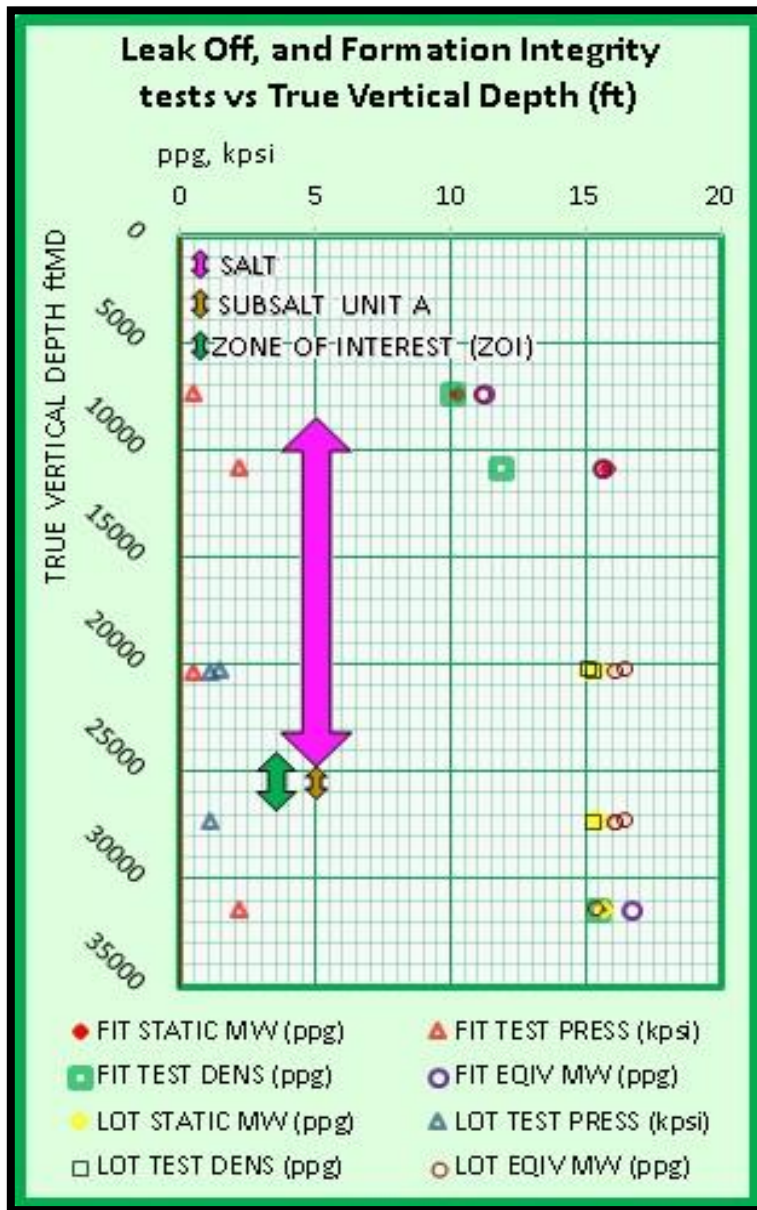
pressure will force fluids into the formation (Leak Off) by fracturing solid rock or by utilizing permeable conduits in the rock. LOT results dictate the mud-regime during drilling. During LOT's formation breakdown, pressure is higher than the pressure at which the fissures close again. In the hydraulic fracturing (fracking) community, fracture gradient is defined as ISIP, also known as Minimum Fracture Extension Pressure and Instantaneous Shut-In Pressure (figure 29).

The unit of measure for resistivity is the ohm-m. The resistivity can take a wide range of values and is usually on a logarithmic scale. This log is a fundamental formation evaluator because the conductive properties of many materials below the surface are distinguishable. For instance, hydrocarbons do not conduct electricity while all formation waters do, so there is a large difference between formations whose pore space is filled with hydrocarbons versus ones filled with formation water. Clay minerals (among others) conduct electricity, reducing the difference. Resistance measurements in a borehole can be used to pick lithological changes, for gathering information about the constitution of a formation, and when combined with porosity measurements, to obtain values of water saturation. This information helps to evaluate the productivity of a formation. Tiber Well shows good separation of resistivity curves from 25,650 ft to 26,050 ft with high readings in the intermixed shale, marl, and sandstone.

Some of the key properties studied in petrophysics are lithology, porosity, water saturation, permeability and density. A key aspect of petrophysics is measuring and evaluating these rock properties by acquiring well log information. When evaluating a reservoir, parameters such as permeability, porosity, and the presence of hydrocarbons are key concerns. Porosity is the crucial parameter for quantifying volumes, and there are various ways to produce accurate porosity data while remaining focused on understanding the reservoir. There are three main

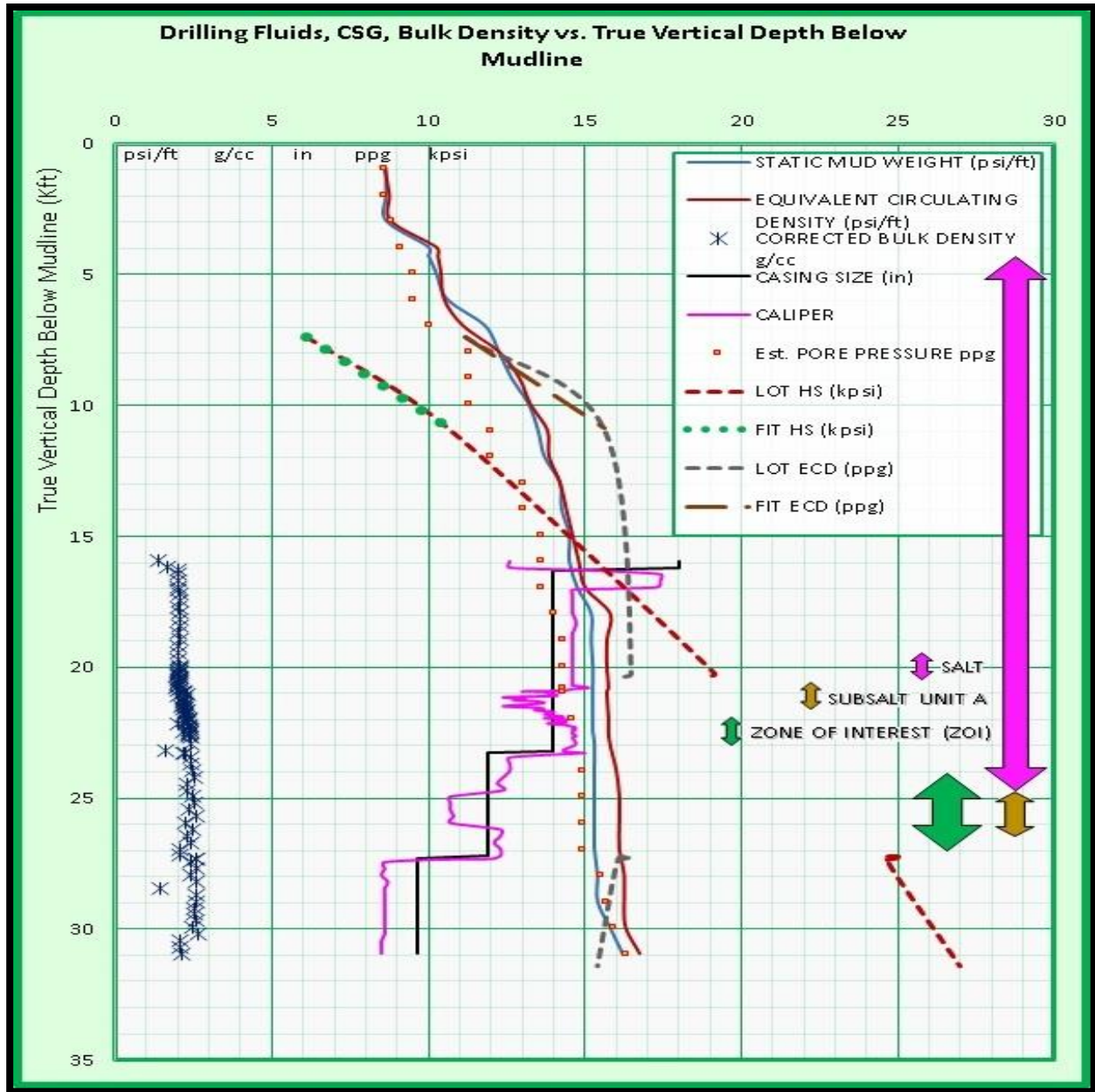
types of porosity logs (none of which take measurement of porosity directly); Acoustic logs, Neutron logs, and Density logs. Certain combinations of these logs provide indicators for lithology, adding more accuracy to porosity estimates. Acoustic logs measure the interval transit time (Δt) of a compressional sound wave travelling through the formation along the axis of the borehole. Acoustic interpretation can yield data including porosity, lithological identifications (when with density and/or neutron logs), synthetic seismograms and mechanical properties of a formation (when with density logs), abnormal formation pressure identification, permeability, and cement bond quality. Density logs emit gamma rays from a chemical source (Ce^{137} and Co^{60}) that can interact with electrons of the material in the formation. Density logs can provide porosity and lithological identifications (from a log of photoelectric absorption properties-PEF and/or with Acoustic and/or Neutron), gas indication and shale/clay content (when with Neutron logs), and synthetic seismograms and formation mechanical properties (when with acoustic logs). Neutron logs measure the hydrogen content. In clean shale-free formations, where pore space is filled with water or oil, the neutron log measures liquid-filled porosity. Porosity is displayed directly on this log but when coupled with other logs can create other data like lithology (when with acoustic and density), gas and shale/clay indicator (when with density) and supports correlations in cased holes.

CONCLUSIONS



Graph 8. Leak off Test and Fracture Integrity Test graph. Data compiled from mud-log report. Graph created using MS Excel 2013.

It is the responsibility of the petrophysicist to employ all available information for the analysis of subsurface petrophysical properties and the water-oil-gas contacts. The geopressure analyst is responsible for processing an extensive list of data including well logs, mud-logs, geological, environment, and drilling reports. From these data, a petrophysical investigation into the formation pressures and fracture gradients within the zone of interest was performed. The zone of interest, in this study, begins at 24,000 ft (1,000 ft above BOS) moving down to 27,000 ft (500 ft below base of Unit A)



Graph 9. Composite graph showing drilling fluid pressure gradients, Casing and bit size comparison, Corrected bulk density, Formation integrity and Leak off tests. Salt, Zone of Interest, and Subsalt unit A represented by the Pink, Green, and, Brown arrows (respectively). Graph created using BSEE well log data and MS Excel 2013.

transitioning from salt into the rubble or gouge zone, then another transition from the gouge zone into the underlying formation. The transition through the dirty salt and into Unit A is evident in many of the well log data and graphs. There are many assumptions in log analysis for overpressure. Dirty salt environments add an element of difficulty to the precarious and complex

process of PP identification within the inclusions and the unpredictability of pressures associated with gouge zones exiting the salt base. Rafted sediment blocks usually contain trapped, abnormally high formation pressures. Penetrating this zone during drilling can take on heavy pressure kicks within the salt and loss of circulation at the salt base. If not prepared, the repercussions can be expensive and may lead to several sidetracks and possible location abandonments. Pore pressure analysts and drilling engineers face an exigent task in dirty salt environments. When coupled with exiting through the BOS into an abnormally pressured, and unconsolidated gouge zone of silt, shale, marl and clay, the petrophysicists must manage the (occasional precarious) well log information with great care and attention.

Tiber Well trajectory was drilled through dirty salt into an abnormally pressured gouge zone. The rafted sediment blocks shown on 2-D seismic are correlated with the well log data and contribute to the calculated high PP gradient throughout the salt body and in many ways presented very similarly to the 'Jack Prospect' from Shaker, (2015) pore pressure publication. The high pore pressures at mid-salt lead to casing installations, FIT, and LOT evaluations and measurements. These, when compared with equivalent circulating density, hydrostatic-lithostatic- and overburden-pressure gradients, show the trending fracture gradient relative to the ECD-PWD fan of graph 7. The depth and pressure gradients below mudline (graphs 1 & 7) compare the mud-fan, hydrostatic pressure, LOT pressures, and fracture gradient (Eaton's method). This graph illustrates well the correlation of these critical data providing a good example of the threshold or pressure envelope adhered to in this environment. The LOT's and FIT's (graph 8 and table 6) show the pressure readings throughout the entire wellbore as per the complete drilling report from BSEE. The LOT provides confirmation to the fracture gradient and

formation pressure graphs by indicating the directly measured formation breakdown pressure. Fracture gradient calculations like Eaton's require the use of Poisson's Ratio (ν). ν was calculated, graphed, and applied to fracture gradient calculations. Eaton's fracture gradient formula can be found in the Formulas and Equations section of this work. ν , overburden (OB) stress and hydrostatic (HS) pressure make up the components of Ben Eaton's fracture gradient calculation.

In the pre-drill stages of a prospect, estimating pore pressure gradients at critical depths of operation is anything besides effortless or straightforward. Starting with only seismic data and velocities, derived information allowing for relatively safe and efficient planning of a drilling operation emerges in the form of many of the well log attributes discussed in this study. Once sufficient data is collected for the estimation process to begin, velocities and their derived formation pressures and fracture gradients are applied to build the predrilling model. The data calculated from interval seismic and velocity allows the drilling teams to prepare the mud-weight and casing programs. Calibration of the pre-drilling model should begin when operations commence. This will provide appropriate information for the planning and execution of a safe and successful drilling operation to the exploration objectives.

REFERENCE

- Bartok, P.**, (1993). Pre-breakup geology of the Gulf of Mexico-Caribbean: Its relation to Triassic and Jurassic rift systems of the region. *Tectonics*, 12(2), 441-459. doi:10.1029/92TC01002.
- Bird, D. E., Burke, K., Hall, S. A., & Casey, J. F.**, (2005). Gulf of Mexico tectonic history: Hotspot tracks, crustal boundaries, and early salt distribution. *AAPG Bulletin*, 89(3), 311-328. doi:10.1306/10280404026.
- BOEM Map Reference**, <http://www.boem.gov/Maps-and-GIS-Data/>.
- Bryant, W. R., Bryant, J. R., Feeley, M. H., & Simmons, G. R.**, (1990). Physiographic and bathymetric characteristics of the continental slope, northwest Gulf of Mexico. *Geo-Marine Letters*, 10(4), 182-199.
- Buffler, R. T., & Sawyer, D. S.**, (1985). Distribution of crust and early history, Gulf of Mexico basin. *Gulf Coast Association of Geological Societies Transactions*. V. 35, 333-344.
- Cazes, C. A.**, (2004). *Overlap Zones, Growth Faults, and Sedimentation: Using High Resolution Gravity Data, Livingston Parish, LA* (Doctoral dissertation, Faculty of the Louisiana State University and Agricultural and Mechanical College in partial fulfillment of the requirements for the degree of Master of Science in The Department of Geology and Geophysics by Carrie Alison Cazes Bachelor of Science in Geology, Louisiana State University).
- Diegel, F. A., Karlo, J. F., Schuster, D. C., Shoup, R. C., & Tauvers, P. R.**, (1995). Cenozoic structural evolution and tectono-stratigraphic framework of the northern Gulf Coast continental margin in M. P. A. Jackson, D. G. Roberts, and S. Snelson, eds., *Salt tectonics: a global perspective: AAPG Memoir 65*, 109-151.
- Dooley T.P., Hudec M.R., Jackson, M.P.A.**, (2012). The Structure and Evolution of Sutures in Allochthonous Salt. *AAPG bulletin*, 96(6), 1045-1070.
- Dribus J.R., Jackson M.P.A., Kapoor J., & Smith M.F.**, (2008, autumn). The Prize Beneath the Salt: Exploration and production activities in the deep and ultradeep waters of the northern Gulf of Mexico [...]. *Oilfield Review*, 4-17.
- Eaton, B. A.**, (1969). Fracture gradient prediction and its application in oilfield operations. *Journal of petroleum technology*, 21(10), 1-353.
- Fiduk, J. C., Weimer, P., Trudgill, B. D., Rowan, M. G., Gale, P. E., Phair, R. L., Korn, B.E., Roberts, G.R., Gafford, W.T., Lowe, R.S., & Queffelec, T. A.**, (1999). The Perdido fold belt, northwestern deep Gulf of Mexico, part 2: seismic stratigraphy and petroleum systems. *AAPG bulletin*, 83(4), 578-612.
- Geologic time scale**, <http://www.geo.ucalgary.ca/~macrae/timescale/timescale.html>. (2016, May).
- Hantschel, T., & Kauerauf, A. I.**, (2009). Pore pressure, compaction and tectonics. In *Fundamentals of Basin and Petroleum Systems Modeling* (pp. 31-101). Springer Berlin Heidelberg.
- House, W., & Pritchett, J. A.**, (1995). Fluid migration and formation pressures associated with allochthonous salt sheets in the northern Gulf of Mexico. In *Salt, sediment and hydrocarbons: Proceedings of the 16th Annual Bob F. Perkins Research Conference, Gulf Coast Section SEPM Foundation* (pp. 121-124).

Hudec, M. R., & Jackson, M. P., (2006). Advance of allochthonous salt sheets in passive margins and orogens. *AAPG bulletin*, 90(10), 1535-1564.

Humphris Jr, C. C., (1978). Salt Movement on Continental Slope, Northern Gulf of Mexico: 2. The Concepts. *AAPG Bulletin* V. 63 1979, issue 5, pp 782-798.

Jackson, C. A. L., Gawthorpe, R. L., Leppard, C. W., & Sharp, I. R., (2006). Rift-initiation development of normal fault blocks: insights from the Hammam Faraun fault block, Suez Rift, Egypt. *Journal of the Geological Society*, 163(1), 165-183.

Jackson, J. A., (1997). *Glossary of geology*, American Geological Institute, Alexandria, VA; 769p. ISBN 0-922152-34-9.

Jackson, M. P., Vendeville, B. C., & Schultz-Ela, D. D., (1994). Structural dynamics of salt systems. *Annual Review of Earth and Planetary Sciences*, 22, 93-117.

Jackson, M. T., & Talbot, C. J., (1986). External shapes, strain rates, and dynamics of salt structures. *Geological Society of America Bulletin*, 97(3), 305-323.

Klien, C., Dutrow, B., & Dana, J. D., (2008). The 23rd ed. of the *Manual of Mineral Science*.

Lee, G. H., Watkins, J. S., & Bryant, W. R. (1992). Origin and Evolution of Keathley Canyon, Northwestern Gulf of Mexico: Chapter 20: Sea Level and Seismic Stratigraphic Studies.

Mancini E.A., Puckett T.M., (2005). Jurassic and Cretaceous Transgressive-Regressive Cycles, Northern Gulf of Mexico, USA. *Stratigraphy*, V.2 No1, pp31-48.

N.O.A.A. bathymetric maps, <http://maps.ngdc.noaa.gov/viewers/bathymetry/>.

PetroWiki; petrowiki.org.

Pindell, J. L., & Kennan, L.,(2007, December). Rift models and the salt-cored marginal wedge in the northern Gulf of Mexico: implications for deep water Paleogene Wilcox deposition and basinwide maturation. In *Perkins Research Conference Proceedings* (Vol. 27, pp. 146-186).

Pindell, J. L., (1994). Evolution of the Gulf of Mexico and the Caribbean. *Caribbean geology: an introduction*, 13-39.

Radovich, B. J., Moon, J., Connors, C. D., & Bird, D., (2007). Insights into structure and stratigraphy of the northern Gulf of Mexico from 2D pre-stack depth migration imaging of mega-regional onshore to deep water, long-offset seismic data.

Saleh, S., Williams, K.E., & Rizvi, A. (2013, September). Rubble Zone Below Salt: Identification and Best Drilling Practices. In SPE Annual Technical Conference and Exhibition. Society of Petroleum Engineers.

Salvador, A., (1987). Late Triassic-Jurassic paleogeography and origin of Gulf of Mexico basin. *AAPG Bulletin*, 71(4), 419-451.

Schlische, R. W., & Anders, M. H., (1996). Stratigraphic effects and tectonic implications of the growth of normal faults and extensional basins. *SPECIAL PAPERS-GEOLOGICAL SOCIETY OF AMERICA*, 183-203.

Schlumberger Oilfield Glossary, <http://www.glossary.oilfield.slb.com/Terms/s/s-wave.aspx>.

Scotese, C.R., (2001). Atlas of Earth History, Volume 1, Paleogeography, PALEOMAP Project, Arlington, Texas, p. 52

Shaker, S. S., (2001). Geopressure Compartmentalization in Keathley Canyon Deep Water, Gulf of Mexico. *Gulf Coast Association of Geological Societies Transactions*, v.LI, p. 293-304.

Shaker, S. S., (2015). A New Approach to Pore Pressure Predictions: Generation, Expulsion, and Retention Trio—Case Histories from the Gulf of Mexico. *Canadian Society for Exploration Geophysicist Recorder*. Jan.2005.

- Shaker, S.S.**, (2008). The Double Edged Sword: The Impact of the Interaction between Salt and Sediment on Subsalt Exploration Risk in Deep Water. *Gulf Coast Association of Geological Societies Transactions*, v. 58, p. 759-769.
- Shaker, S.S.**, (2009). Dirty vs. Clean Salt: Their Impact on the Subsalt Wilcox Deepwater Exploration Plays. *Gulf Coast Association of Geological Societies Transactions*, v. 59, p. 689-698.
- Stern, R. J. & Dickinson, W. R.**, (2010). The Gulf of Mexico is a Jurassic backarc basin. *Geosphere*, 6(6), 739-754.
- Trudgill, B. D., Rowan, M. G., Fiduk, J. C., Weimer, P., Gale, P. E., Korn, B. E., Phair RI, Gafford W.T., & Dobbs, S. W.**, (1999). The Perdido Fold Belt, Northwestern Deep Gulf of Mexico, Part 1: Structural Geometry, Evolution and Regional Implications1. *AAPG bulletin*, 83(1), 88-113.
- Vendeville, B. C., & Jackson, M. P. A.**, (1992). The fall of diapirs during thin-skinned extension. *Marine and Petroleum Geology*, 9(4), 354-371.
- Vendeville, B. C., & Jackson, M. P. A.**, (1992). The rise of diapirs during thin-skinned extension. *Marine and Petroleum Geology*, 9(4), 331-354.
- Wu, S., Bally, A. W., & Cramez, C.**, (1990). Allochthonous salt, structure and stratigraphy of the northeastern Gulf of Mexico. Part II: Structure. *Marine and Petroleum Geology*, 7(4), 334-370.
- Yan, F., Han, D. H., Yao, Q., & Li, H.**, (2014, October). Seismic velocities of halite salt: anisotropy, dispersion, temperature and stress effects. In 2014 SEG Annual Meeting. Society of Exploration Geophysicists.
- Young, R. A., & Lepley, T.** (2005). Five Things Your Pore Pressure Analyst Won't Tell You. American Association of Drilling Engineers; National Technical Conference and Exhibition.
- Young, R. A., & Lepley, T.**, (2005). Five Things Your Pore Pressure Analyst Won't Tell You. *American Association of Drilling Engineers*.
- Zhang, J.**, (2011). Pore pressure prediction from well logs: Methods, modifications, and new approaches. *Earth-Science Reviews*, 108(1), 50-63.

EQUATIONS

- Fracture gradient: the bottom-hole pressure gradient required to initiate or extend a fracture. Fracture pressure gradient is a function primarily of overburden stress gradient, pore pressure gradient, and the ratio of horizontal to vertical stress.

- Ben Eaton formula (F):** Overburden load, Poisson's ratio for rocks, and pressure gradients vary with depth. This method developed specifically for the Gulf Coast. 1969.

$$F = \left(\frac{S-P}{D}\right) \left(\frac{\gamma}{1-\gamma}\right) + \frac{P}{D}$$

F = Fracture gradient (psi/ft)

$\frac{S}{D}$ = Overburden stress gradient (psi/ft)

$\frac{P}{D}$ = Pore pressure gradient (hydrostatic pressure) (psi/ft)

γ = Poisson's Ratio

- Hubbert & Willis formula ($F_{\min/\max}$):** Overburden stress gradient, formation pore-pressure gradient and Poisson's ratio of rocks were the independent variables that were shown to control fracture pressure gradient, the dependent variable. 1957.

$$F_{\min} = \frac{1}{3} \left(1 + \frac{2P}{D}\right) \quad F_{\max} = \frac{1}{2} \left(1 + \frac{P}{D}\right)$$

F = Fracture gradient (psi/ft)

$\frac{P}{D}$ = Pore pressure gradient (psi/ft)

- Matthews & Kelly formula (F):** Developed the concept of variable ratio between the effective horizontal and vertical stresses. Stress ratios increase according to the degree of compaction. 1967.

$$F = \frac{K_i \sigma}{D} + \frac{P}{D}$$

K_i = Matrix stress coefficient

σ = Vertical matrix stress (psi/ft)

- Hydrostatic pressure (pore pressure) gradient formula (Ph):** Formation fluid pressure at depth.

$$Ph = ((W_{\text{mud}})(0.052))(d_{\text{ml}})$$

Ph = Hydrostatic pressure

W_{mud} = Drilling mud-weight (ppg)

d_{ml} = depth below mudline

0.052 = commonly used conversion constant derived by this dimensional analysis:

$$\frac{1 \text{ psi}}{\text{ft}} \times \frac{1 \text{ ft}}{12 \text{ in}} \times \frac{1 \text{ lb/in}^2}{1 \text{ psi}} \times \frac{2.31 \text{ in}^3}{1 \text{ US Gal}} = 19.25 \text{ lb/gal} \quad 19.25^{-1} = 0.05195$$

3. Hydrostatic pressure (pore pressure) formula (ρ): Formation fluid pressure produced by a column of fluid extending to the surface.

$$p = h \rho g$$

p = pressure (psi/ft)

h = height of fluid column at which the pressure is measured (m, in)

ρ = density of liquid (mud-weight ppg)

g = the gravitational constant (9.81 m/s², 32.17405 ft/s²)

4. Gardner-Gardner relation (ρ): The empirical relationship that density is proportional to the $\frac{1}{4}$ power of P-wave velocity. (The relationship of seismic P-wave velocity to the bulk density of the lithology in which the wave travels.) α and β are empirically derived constants dependent upon the geology. Gardner et al. 1974, proposed that a good fit can be obtained by taking $\alpha = 0.23$ and $\beta = 0.25$.

$$\rho = \alpha V_p^\beta$$

ρ = bulk density (g/cm³)

V_p = P-wave velocity given in (ft/s)

$\alpha = 0.23$ for (ft/s), 0.31 for (m/s)

$\beta = 0.25$

5. Overburden pressure (S): The resultant pressure from material above a refractor or reflector.

$$S = P + \sigma$$

S = Overburden stress (psi)

P = Pore pressure (psi)

σ = matrix stress (psi)

6. Overburden pressure gradient ($\frac{P}{D}$): The sum of overburden stress and matrix stress at depth.

$$\frac{P}{D} = \frac{S}{D} + \frac{\sigma}{D}$$

D = Depth (ft,m)

S = Overburden stress (psi)

σ = Matrix stress (psi)

7. Lithostatic pressure gradient ($p(z)$): The stress imposed on a layer of soil or rock by the weight of overlying material.

$$p(z) = p_0 + g \int_0^z p(z) dz$$

$p(z)$ = density of overlying rock at depth z .

g = acceleration due to gravity.

p_0 = datum pressure at the surface

8. Bulk modulus (K): The stress-strain ratio under simple hydrostatic pressure which measures a substance's resistance to uniform compression.

$$K = M - \frac{4G}{3}$$

M = compressional modulus

G = Shear modulus

9. Shear modulus (G): The stress-strain ratio for simple shear.

$$G = \frac{\alpha \rho b}{(\Delta t_s)^2}$$

α = unit conversion constant

ρb = bulk density

Δt_s = shear slowness time

10. Shear velocity (Vs):

$$V_s = \sqrt{\frac{G}{\rho}}$$

G = Shear modulus

ρ = bulk density

11. Compressional (P-wave) modulus (M): the ratio of axial stress to axial strain in a uniaxial strain state.

$$M = \frac{\alpha \rho b}{(\Delta t_c)^2}$$

α = unit conversion constant

ρb = bulk density

Δt_c = compressional slowness time

12. Compressional (P-wave) velocity (Vc):

$$V_c = \sqrt{\frac{M}{\rho}}$$

M = Compressional modulus

ρ = Bulk density

13. Young's modulus (E): the ratio of the stress along an axis to the strain along that axis in the range of stress in which Hooke's law holds.

$$E = \frac{9KG}{(3K+G)}$$

K = Bulk modulus

G = Shear Modulus

14. Poisson's Ratio (ν): The ratio of the fractional transverse contraction to the fractional longitudinal extension of an elastic solid.

$$\nu = \frac{3K-2G}{6K+2G} \quad \text{or} \quad \nu = \left(\frac{1}{2}\right) \frac{\left(\frac{V_p}{V_s}\right)^2 - 2}{\left(\frac{V_p}{V_s}\right)^2 - 1}$$

K = Bulk modulus

G = Shear modulus

V_p = P-wave velocity

V_s = S-wave velocity

15. Nyquist Frequency (f_N): A frequency associated with sampling which is equal to half the sampling frequency. Frequencies greater than the Nyquist frequency alias as lower frequencies from which they are indistinguishable. This frequency is used to calculate wavelength and vertical resolution from seismic velocity and sample rate.

$$f_N = \frac{1}{2\Delta T} \rightarrow v = \lambda f \rightarrow \frac{\lambda}{4} \rightarrow \text{vertical resolution}$$

ΔT = seismic sample rate

v = velocity

λ = wavelength

f = frequency

$\frac{\lambda}{4}$ = quarter wavelength

16. Acoustic impedance (Z): Seismic velocity multiplied by density. Reflection coefficient at normal incidence depends on changes in acoustic impedance.

$$Z = \rho(V_c)$$

ρ = bulk density

V_c = compressional (P-wave) velocity

17. Reflection coefficient (Γ): The energy or wave from a seismic source which has been reflected (returned) from an acoustic impedance contrast (reflector) or series of contrasts within the earth. A ratio of resistivities.

$$\Gamma = \frac{Z_L - Z_S}{Z_L + Z_S}$$

Z_L = load impedance

Z_S = source impedance

VITA

The author is originally from Lake Charles, Louisiana, graduating from Sam Houston High School in Lake Charles, Louisiana, in 1994. After graduation, he began working in local refineries and chemical plants. In 1996, he moved to Baton Rouge, Louisiana in pursuance of a trade school certification from ITI Technical College in Industrial Instrumentation and Controls Systems Technology. After graduating with certification, he entered the petro-chemical workforce as a process controls specialist.

The author attained the degree Bachelor of Science from the University of New Orleans in Petroleum Geology in 2013. In 2014, he rejoined the Earth & Environmental Sciences department as a graduate research assistant continuing his education in seismic interpretation and geophysics under the direction of Dr. A.K.M. Sarwar.